Evaluation of Micromixing Models for Turbulent Mixing in Supercritical Water

M. Koene

to obtain the degree of Bachelor of Science

at the Delft University of Technology,

to be defended publicly on Wednesday July 11, 2018 at 10:00 AM.

Student number:	4452925	
Project duration:	July 28, 2017 – July 11, 2018	
Thesis committee:	Prof. Dr. D.J.E.M. Roekaerts,	TU Delft, supervisor
	Prof. Dr. Ir. A.W. Heemink,	TU Delft, supervisor
	Prof. Dr. F.H.J. Redig,	TU Delft
	Dr. Ir. R. Pecnik,	TU Delft

TU Delft

Abstract

Hydrothermal flames have become a very important field of study, especially for supercritical water oxidation. In supercritical water oxidation hazardous, toxic or non-biodegradable aqueous organic waste water streams can be efficiently destructed. Supercritical water oxidation takes place in a aqueous environment above the supercritical point.

In the case of turbulent flow, micromixing models are needed. In this work, three different mixing models are analysed in a hydrothermal flame environment. These models are Interaction by Exchange with the Mean, Coalescence/Dispersion and the Mapping Closure model. When the mixing is done around temperatures far below or far above the pseudocritical temperature all models gave the same evolution of average temperature. However when the mixing is done around the pseudocritical temperature the differences are large. The Mapping Closure model is best in agreement with the Navier-Stokes equations so it is advised to use that model when simulating mixing around the pseudocritical temperature.

Contents

Introduction

Hydrothermal flames have become a very important field of study, mostly for the practical applications of supercritical water oxidation for the efficient treatment of hazardous, toxic, or non-biodegradable aqueous organic waste water streams. [14] Supercritical water oxidation takes place in a aqueous environment above the supercritical point. At these conditions fuel can be mixed inside the water.

Numerical model studies of hydrothermal flames can save money and time provided the models are validated using data from experiments or detailed reference simulations. Simulation of these hydrothermal flames is done using reaction equations and mixing processes. Modelling a mixing process using the Navier-Stokes equations can be quite difficult and it comes along with long computation time. A different approach is to use micromixing. At micromixing the positions of individual particles is not taken into account for the reason that in high turbulent fields the mixing is better determined using stochastic processes. In hydrothermal flame environments, there is a lot of turbulence, that is why micromixing models are excellently suited for these situations. In this report three different micromixing models are analysed in the case of hydrothermal flames. These models are Interaction by Exchange with the Mean, Coalescence/dispersion and the Mapping Closure model. For these models the time evolution of the mixing, of water at temperatures corresponding to temperatures in hydrothermal flames, is compared and discussed. The goal of this report is to check whether the different models give the same results as the Navier-Stokes equations or not in the special case of hydrothermal flames.

In the first part of the report information about hydrothermal flames is given. After that the properties of supercritical water, which is the environment of hydrothermal flames, is explained and with that different properties of water around the critical temperature will be shown using plots.

In the second part the three mixing models will be given together with a derivation of how they work when implemented with particles. Also some plots which give insight about how these models work is added in this part. At the end of this part a discussion about the differences in models is given.

In the third part the program which does all calculations is explained. In the fourth part the results are given, accompanied by a discussion about these results. Finally a conclusion is given.

This report is part of the requirements for the degree of Bachelor of Science in Applied Physics and Applied Mathematics.

1 Background

1.1. Hydrothermal flames

Hydrothermal flames are rapid oxidation reaction inside a supercritical aqueous environment.[3] The temperatures and reaction rates are sufficient to produce luminous flames. What supercritical water is will be discussed in section 1.2. Just like in combustion a fuel and an oxidizer are required for a burning process. The fuel, for example methane or methanol, is dissolved in the water and a oxidant stream of air or oxygen is mixed with the solution. When fuel and oxidizer are fully mixed and when the temperature is high enough spontaneous ignition will occur. The fuel water solution is flexible because it can flow in a similar way to water. After the reactions the combustion products flow with the water. This makes it easier to handle the hazardous reaction products. Hydrothermal flame reactors can be used to efficiently clean wastewater streams. This is done by using the high temperatures in the reactor to destroy organic compounds inside the water. ETH Zurich has designed multiple hydrothermal burners. A schematic of one of them, which is called the coaxial burner, is shown in figure 1.1 below. [11]

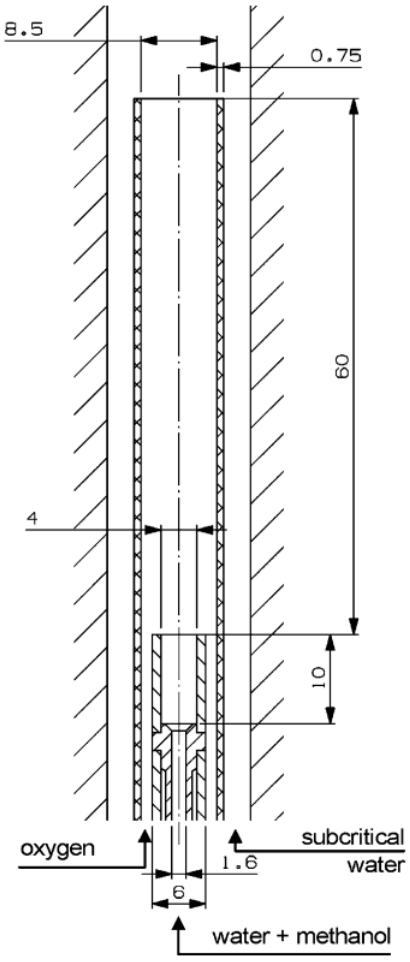

Figure 1.1: Schematic of a coaxial burner. The lengths are measured in mm

A mixture of water and methanol flows into the center of the reactor. Oxygen is added with a coaxial flow around the fuel. Around that is a coaxial wall with a counterflow of subcritical water. This cools the reactor down and protects the outer walls.

1.2. Supercritical water

Supercritical water is ordinary water at a supercritical phase. This supercritical state occurs above a certain high temperature and a certain high pressure, this is called the critical point. For water this critical point has a temperature of 374 $^{\circ}C$ (or 647 K) and a pressure of 221 bar. [6] The full phase diagram for water is shown in figure 1.2. An important curve in this figure is the liquid-vapour curve, above this curve water behaves like a liquid or a solid depending on the temperature and pressure. Below and to the right of this curve the water behaves like a gas. The critical point is located at the end of this curve. For temperatures and pressures above the critical point, a fluid behaves differently and has different properties compared to the gas or liquid phase.

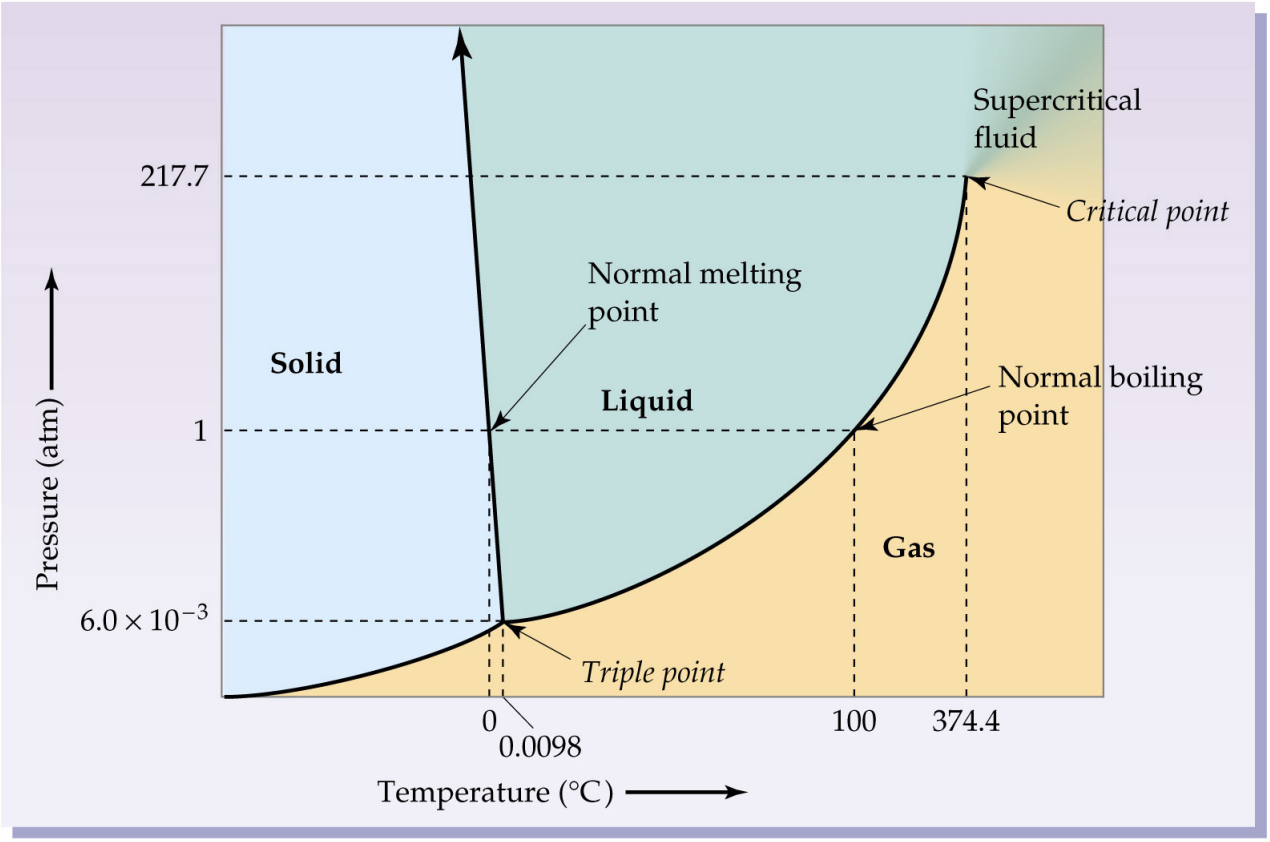

Figure 1.2: Phase diagram for water. [2]

In this report the pressure is 250 bar, which is above the critical pressure and is also used multiple times in the experiments of ETH Zurich. At this pressure the water is either in a solid state, at liquid state or in the supercritical state. The temperatures used in hydrothermal flame environments are much higher than the melting point, so solid water, also known as ice, will not have a role in this report. The important part is the transition between the liquid and the supercritical phase. For pressures above the critical pressure, the transition where a rapid change of properties occur is at a different temperature than the critical temperature. This is called the pseudocritical temperature. The pseudocritical temperature is defined at the point where the heat capacity has its peak value.

In the next part the pseudocritical temperature is found using the heat capacity and some other properties are plotted against the temperature. The data is taken from the REFPROP databases made by the National Institute of Standards and Technology (USA) (NIST). [5] In all cases the pressure is taken to be at 250 bar.

In figure 1.3 the maximum of the heat capacity is located at 663 K which is indeed higher than 647 K found before. So that means that at a pressure of 250 bar the pseudocritical temperature is 663 K.

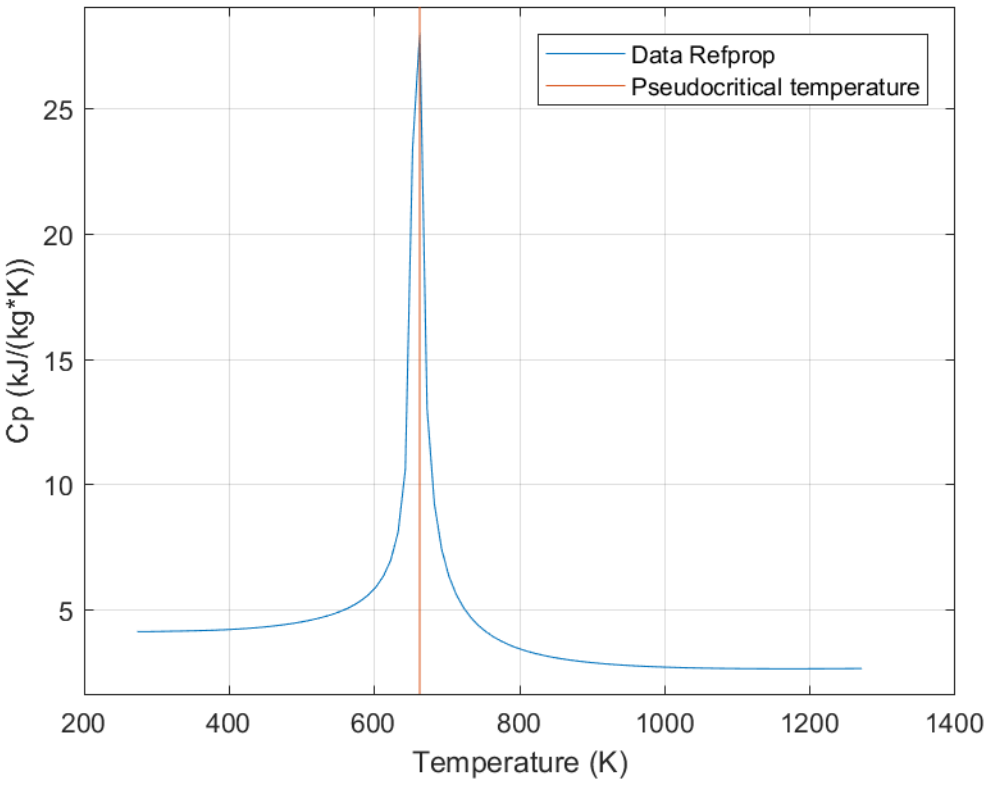

Figure 1.3: Specific heat capacity of water at 250 bar for different temperatures around the critical temperature.

The density decreases a lot when getting close to the pseudocritical temperature, this is shown in figure 1.4.

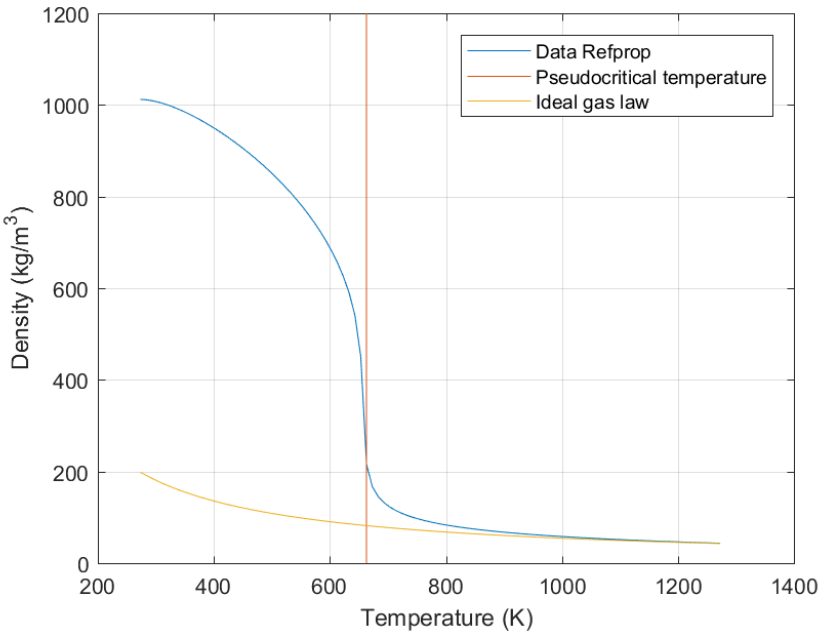

Figure 1.4: Density of water at 250 bar for different temperatures around the critical temperature. Also the Ideal gas law is plotted for water.

The density slowly decreases when the temperature approaches the pseudocritical temperature, but drops really fast to 200 kg/m^3 at the pseudocritical temperature. This indicates that for lower temperatures the water behaves like a liquid, but above the pseudocritical temperature the curve approaches the ideal gas law. The viscosity has a significant drop below the pseudocritical temperature and drops even more at the pseudocritical temperature. For higher temperatures the viscosity slowly increases. A graph of the viscosity is shown in figure 1.5.

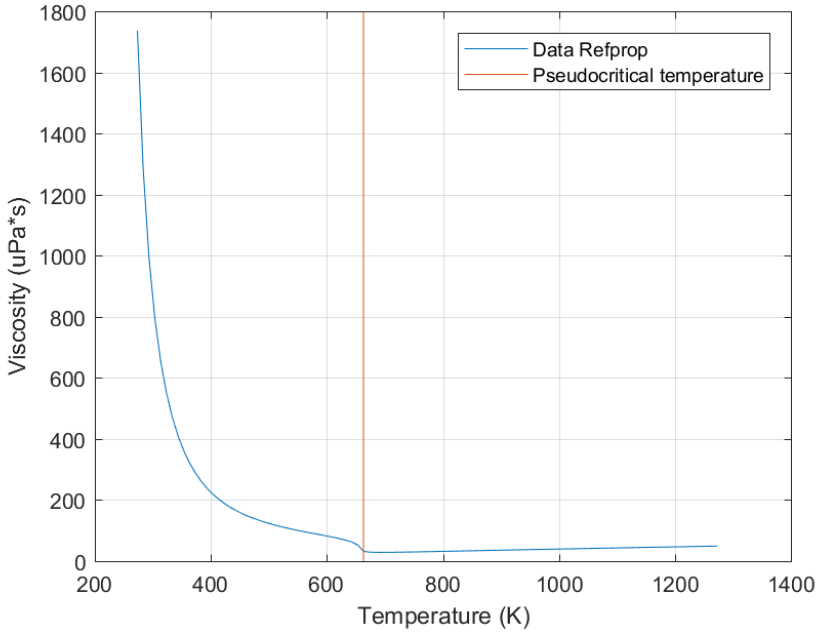

Figure 1.5: Viscosity of water at 250 bar for different temperatures around the critical temperature.

A figure of the specific enthalpy for different temperatures is shown in 1.6 below. Note that this function monotone increasing.

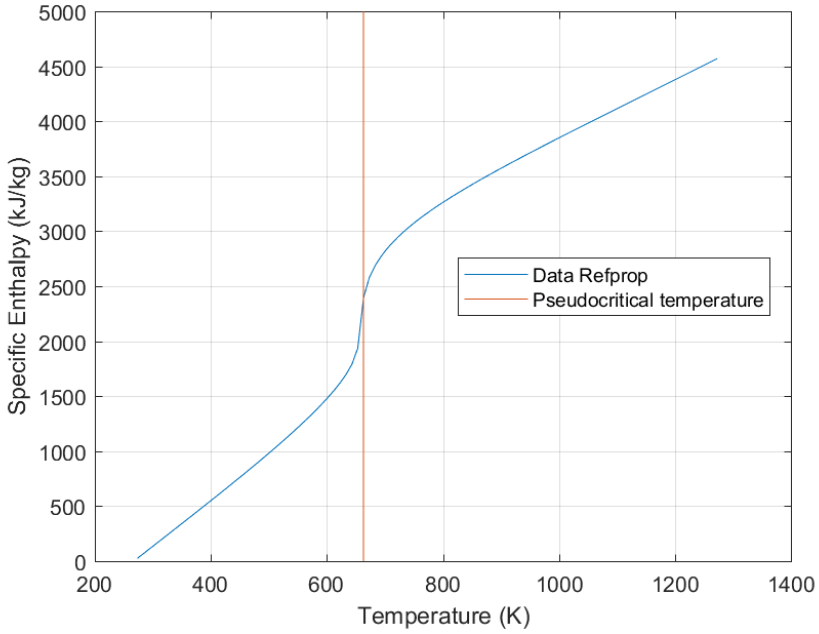

Figure 1.6: Specific Enthalpy of water at 250 bar for different temperatures around the critical temperature.

The specific enthalpy increases linearly for low temperatures until it reaches the pseudocritical temperature. Then the specific enthalpy jumps really fast and after that it increases linearly again.

The thermal conductivity reaches its maximum around 400 K, for higher temperatures the thermal conductivity drops. The fastest decrease is around the pseudocritical temperature. After that the thermal conductivity increases with temperature. This is shown in figure 1.7

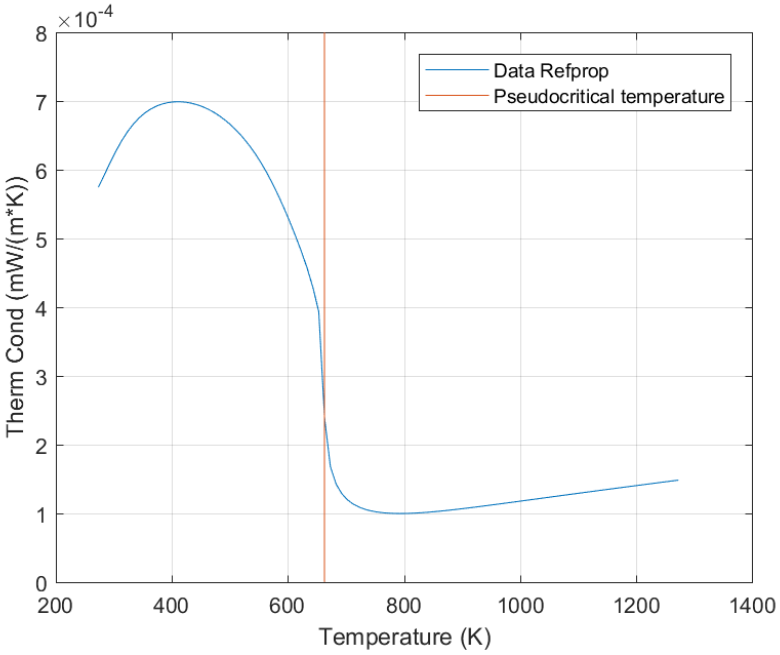

Figure 1.7: Thermal conductivity of water at 250 bar for different temperatures around the critical temperature.

2

Micromixing Models

2.1. Interaction by Exchange with the Mean

The focus in this report is on turbulent diffusion flames. Micromixing models are well suited for turbulent flows. Micromixing describes how small particles or mass elements mix with each other without changing the individual locations. A particle represents a specific amount of mass. Volume can be obtained by using the density. The properties considered are scalar properties, with some of them per unit mass. In particular the enthalpy per unit mass or specific enthalpy.

A widely known mixing model is called Interaction by Exchange with the Mean or IEM. This model is also known as Linear Mean-Square Estimation or LMSE. Deviation from the mean is the only driving force considered in this model. [13] The differential equation for a scalar ψ is given by [4]

$$\frac{d\psi(t)}{dt} = -\frac{c\omega}{2}(\psi(t) - \langle\phi\rangle) \tag{2.1}$$

where c is a mixing model constant, which is determined by comparing with experiments. The value of c is usually taken as 2.0 to have the desired scalar variance decay rate. [15] ω is in turbulent mixing defined as the mean turbulence frequency calculated by

$$\omega = \frac{\epsilon}{k} \tag{2.2}$$

ϵ and k come from the $(k-\epsilon)$ turbulence model, k is the kinetic energy of turbulent velocity fluctuations and ϵ is the dissipation rate of turbulent kinetic energy. A derivation of k and ϵ is available in (Launder and Spalding)[8]. $\langle\phi\rangle$ is called the Favre average which is the average of ϕ weighted with the density. $\psi^{(j)}$ is defined as the scalar ψ corresponding to particle j. When all particles represent the same amount of mass and when there are N particles, the average can be calculated with a sum resulting in.

$$\langle\phi\rangle = \frac{1}{N}\sum_{j=1}^{N}\psi^{(j)} \tag{2.3}$$

Combining this with (2.1) results in:

$$\frac{d\psi(t)}{dt} = -\frac{c\omega}{2}\left(\psi(t) - \frac{1}{N}\sum_{j=1}^{N}\psi^{(j)}(t)\right) \tag{2.4}$$

The average is constant in the IEM model so the average at time t is equal to the average at the starting time of the mixing process t_0. The solution of (2.4) is given by:

$$\psi^{(i)}(t) = e^{-\frac{c\omega}{2}(t-t_0)}\psi^{(i)}(t_0) + \left(1 - e^{-\frac{c\omega}{2}(t-t_0)}\right)\frac{1}{N}\sum_{j=1}^{N}\psi^{(j)}(t_0) \tag{2.5}$$

The derivation of this can be found in appendix A.1. Evolution of the scalars $\psi^{(i)}$ is fully determined by the starting condition and the average. Because of this the model is easy implementable in various situations. As

result from its simplicity IEM also has some evident flaws. When the difference with the average is large the scalar ψ will move faster to the average. However particles which move faster will never catch up to the slower particles, because if a particle is getting close to a slow moving particle its speed will also decrease to that of the slow moving particle. This statement will lead to an evolution in time where the shape of the distribution stays the same as the starting shape. In other words, two distinct peaks will always stay two distinct peaks, but they will get closer together over time.

In the figures below distributions at different moments in time are shown. Mixing is done using IEM. Z is a scalar which belongs to the particles getting mixed. In the application discussed in chapter 4.1, the physical meaning that can be given to Z is scaled specific enthalpy. This is the enthalpy per unit mass with physical values scaled to fit the interval $[0,1]$.

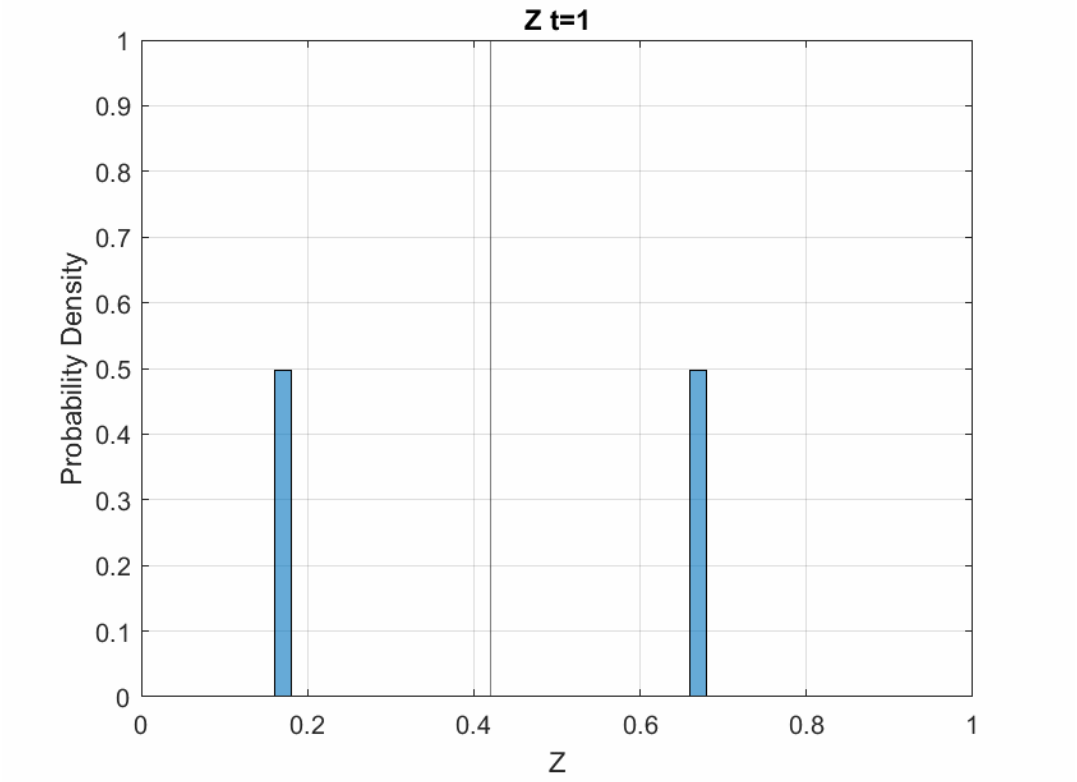

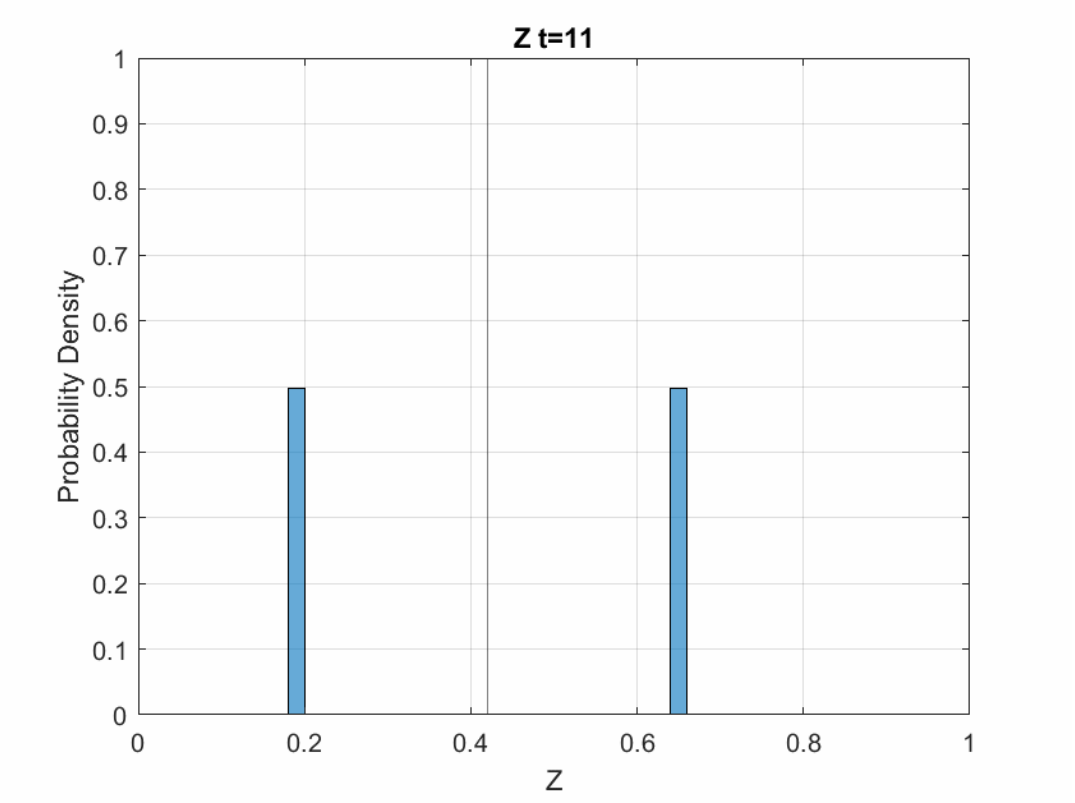
Z t=11
Probability Density
Z
0
0.1
0.2
0.3
0.4
0.5
0.6
0.7
0.8
0.9
1
0.2
0.4
0.6
0.8

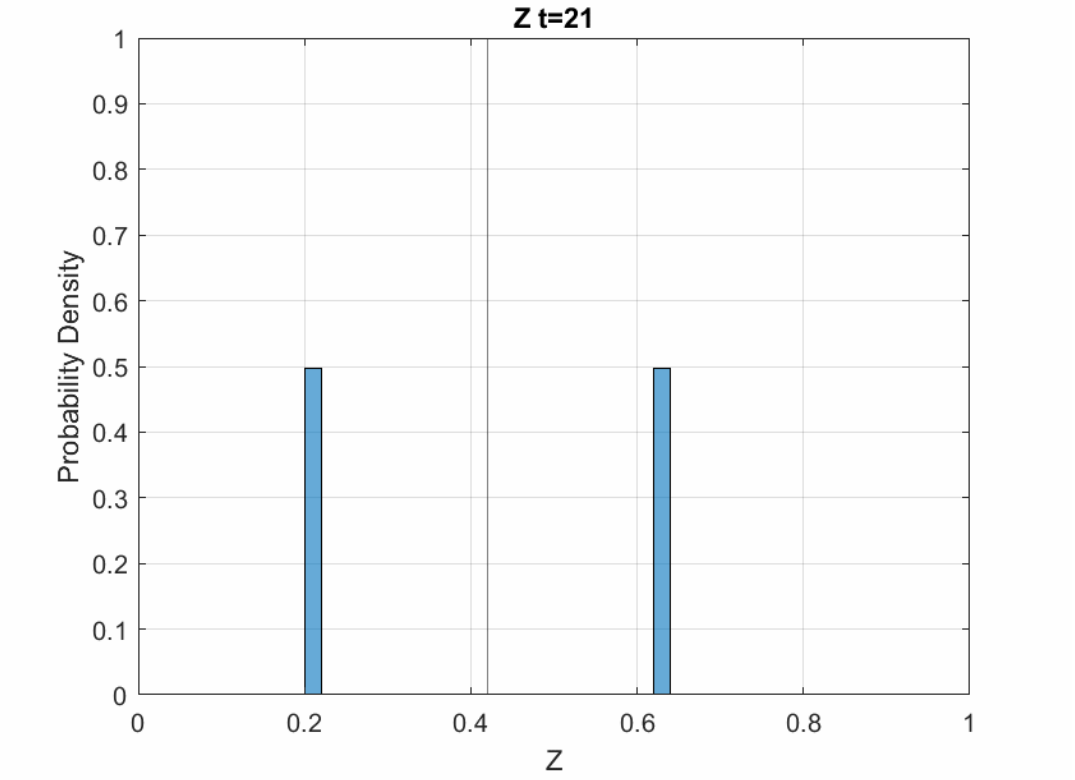
Z t=21
Probability Density
Z
0
0.1
0.2
0.3
0.4
0.5
0.6
0.7
0.8
0.9
1
0.2
0.4
0.6
0.8

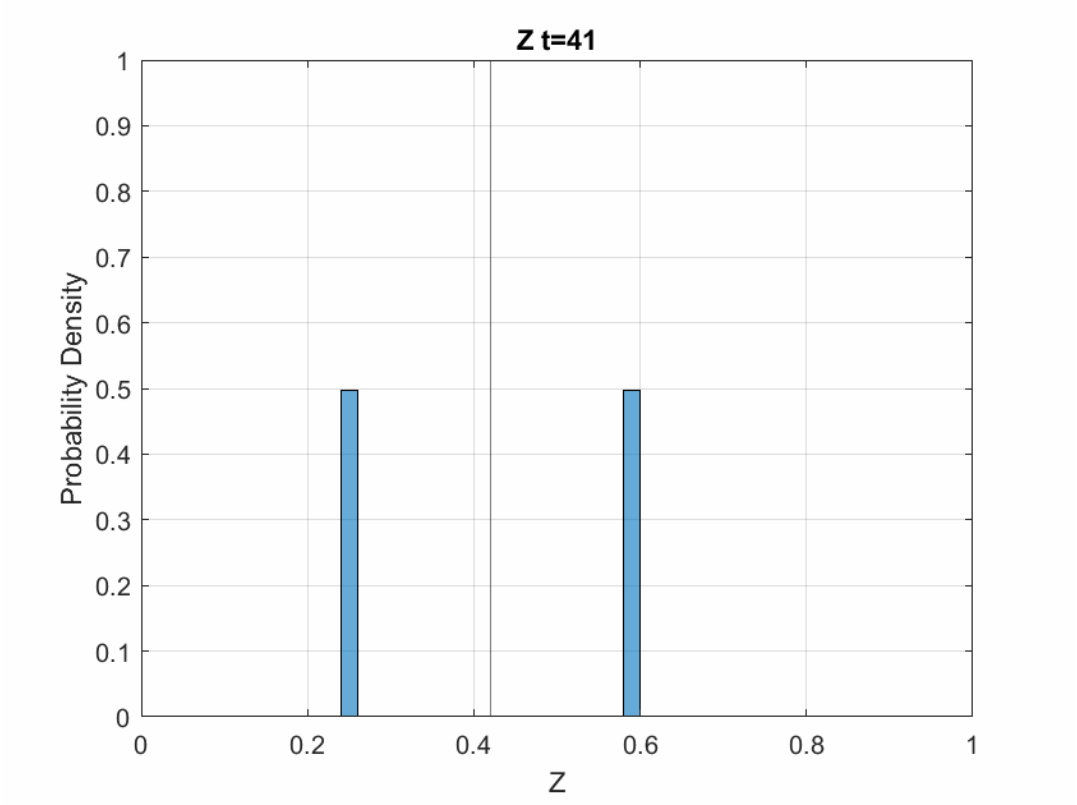
Z t=41
Probability Density
Z
0
0.1
0.2
0.3
0.4
0.5
0.6
0.7
0.8
0.9
1
0.2
0.4
0.6
0.8

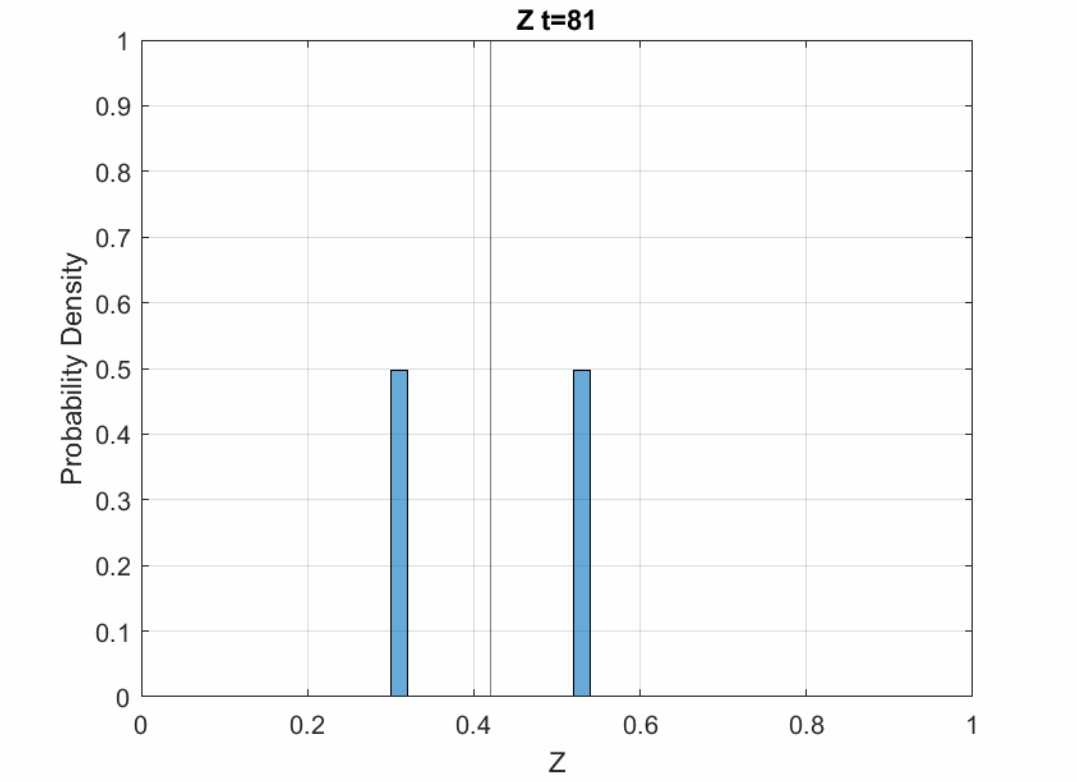
Z t=81
Probability Density
Z
0
0.1
0.2
0.3
0.4
0.5
0.6
0.7
0.8
0.9
1
0.2
0.4
0.6
0.8

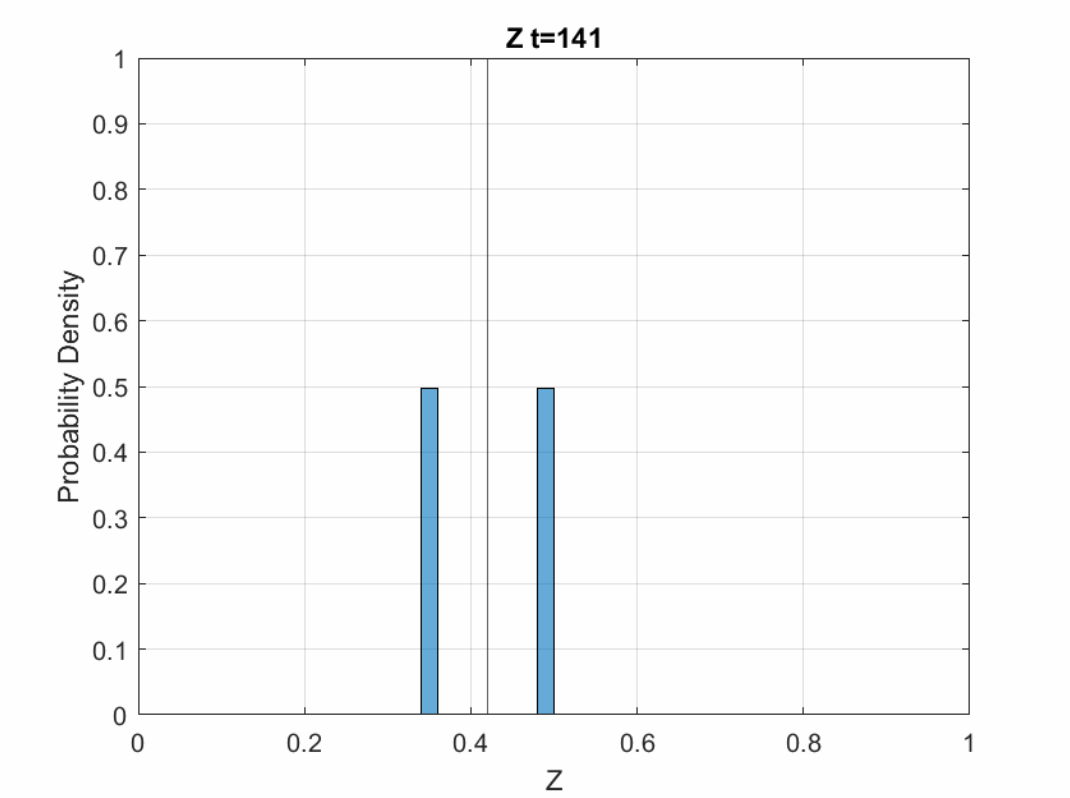
Z t=141
Probability Density
Z
0
0.1
0.2
0.3
0.4
0.5
0.6
0.7
0.8
0.9
1
0.2
0.4
0.6
0.8

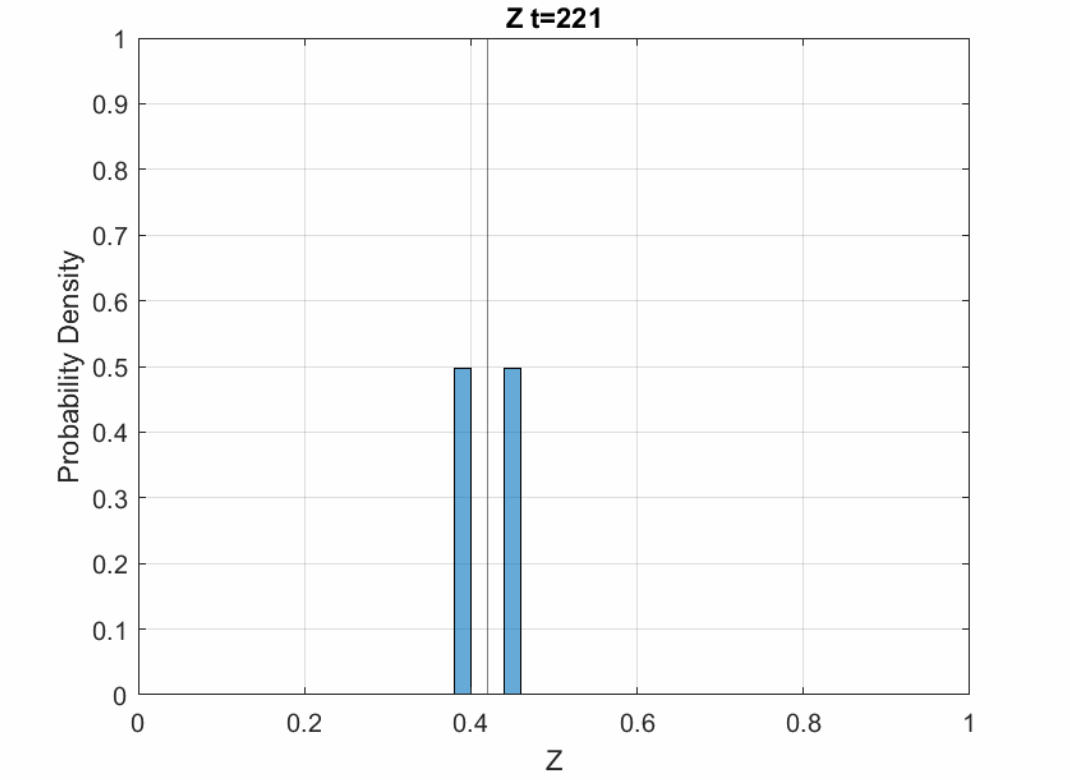
Z t=221
Probability Density
Z
0
0.1
0.2
0.3
0.4
0.5
0.6
0.7
0.8
0.9
1
0.2
0.4
0.6
0.8

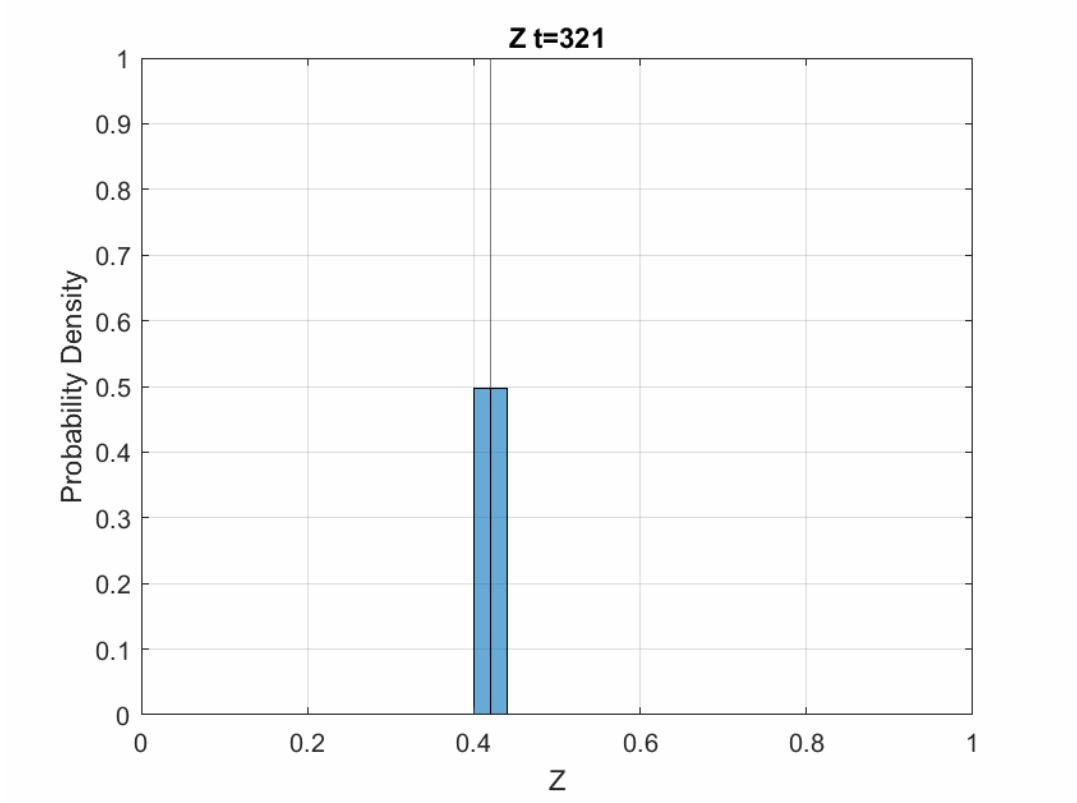

Figure 2.1: Evolution of a PDF using the Interaction by Exchange with the Mean model. The vertical black line indicates the average value.

As written before the two starting peaks move closer over time. Note that the average stays the same over time.

2.2. Coalescence/Dispersion model

The Coalescence/Dispersion model is different from IEM. Instead of particles interacting with the average, particles interact with each other. [13] Therefore information about the full PDF is required to calculate the behaviour over time. One method to define this model is to use a time step Δt. In the time interval $[t, t+\Delta t]$ two particles either mix or none of the particles mix at all. Defining a time scale τ_N as:

$$\tau_N = \frac{\tau}{cN}$$

where c is the same mixing model constant as in the IEM model, N is the number of particles and $\tau = \frac{k}{\epsilon}$. With a probability of $\frac{\Delta t}{\tau_N}$ two different particles mix together. This is done by randomly choosing p and q, those two particles get mixed and the resulting values of the scalars of particle p and q are determined using.

$$\phi^{(p)}(t+\Delta t) = \phi^{(q)}(t+\Delta t) = \frac{1}{2}\left(\phi^{(p)}(t) + \phi^{(q)}(t)\right) \tag{2.6}$$

With a probability of $1 - \frac{\Delta t}{\tau_N}$ all particles stay the same. Another method to define this model is to, instead of 2 particles with probability $\frac{\Delta t}{\tau_N}$, mix more than two particles at the same time. In that case during a time step Δt the amount of particles that mix $n_m = 2\left[\left[\frac{\Delta t}{\tau_N}\right]\right]$. Where $[[x]]$ is a function from $\mathbb{R}$ to $\mathbb{Z}$ which maps the value x to the nearest integer in $\mathbb{Z}$. Since every mixing happens between two particles, there is a 2 in the definition. When applying this method a chosen particle can only mix with one other, implying n_m should be even (which is already the case by rounding and the factor 2) and it should be smaller than N the number of particles in the system.

Both methods are essentially the same, but for a large Δt the first method does not work optimal and for a small Δt the second method does not work optimal. Take for example $\Delta t = 2\tau_N$, than in a time $2\tau_N$ the

probability of mixing is 2 which is larger than 1. Depending on how this is implemented, this can result in 1 mixing pair in a time interval of $2\tau_N$. If on the other hand $\Delta t = \tau_N$ the probability of mixing is 1, so in a time interval of 2τ, 2 time steps have passed meaning in the time interval $2\tau_N$, 2 pairs have mixed. This is not what was supposed to happen considering the time scale did not change. Try the second method with $\Delta t = \frac{\tau_N}{4}$, then $n_m = 2[[\frac{\Delta t}{\tau_N}]] = 2[[\frac{1}{4}\frac{\tau_N}{\tau_N}]] = 2[[\frac{1}{4}]] = 0$. Now no particles would mix at all.

The CoDi model converges to a PDF with a single peak around the average. This is totally different from IEM which showed that two peaks would never converge to a single peak.

One disadvantage of this model is its physical representation. On discrete time points particles would instantaneously change their properties. Also when starting with values 0 and 1, the first time steps will result in scalars with values 0, $\frac{1}{2}$ and 1 and later the scalars will have values of 0, $\frac{1}{4}$, $\frac{1}{2}$, $\frac{3}{4}$, and 1. A modification of this model is made which prevents this last problem from occurring.

The modified version is different in the way how two particles mix together. [12] Instead of getting both the value as defined in (2.6), they get mixed for an amount depending on a random variable α between 0 and 1. If α is 0, the particles stay the same and if α is 1, the particles get fully mixed according to (2.6). Between 0 and 1 the particles change according to:

$$\phi^{(p)}(t+\Delta t) = \frac{1}{2}\alpha\left(\phi^{(p)}(t)+\phi^{(q)}(t)\right)+(1-\alpha)\phi^{(p)} \tag{2.7}$$

and

$$\phi^{(q)}(t+\Delta t) = \frac{1}{2}\alpha\left(\phi^{(p)}(t)+\phi^{(q)}(t)\right)+(1-\alpha)\phi^{(q)} \tag{2.8}$$

This modification ensures that the scalars will not occur in the same distinct points. However this does not solve the problem that only at discrete time point mixing occurs.

In the figures below distributions at different moments in time are shown. Mixing is done using CoDi. Z is a scalar which belongs to the particles getting mixed.

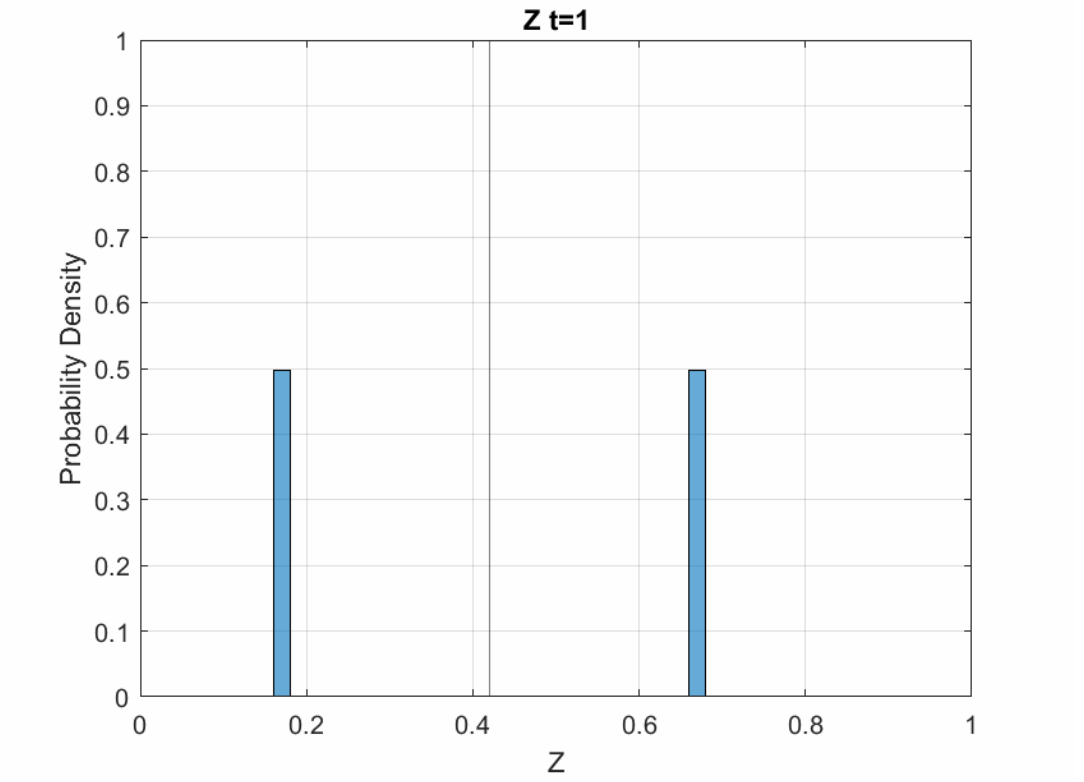

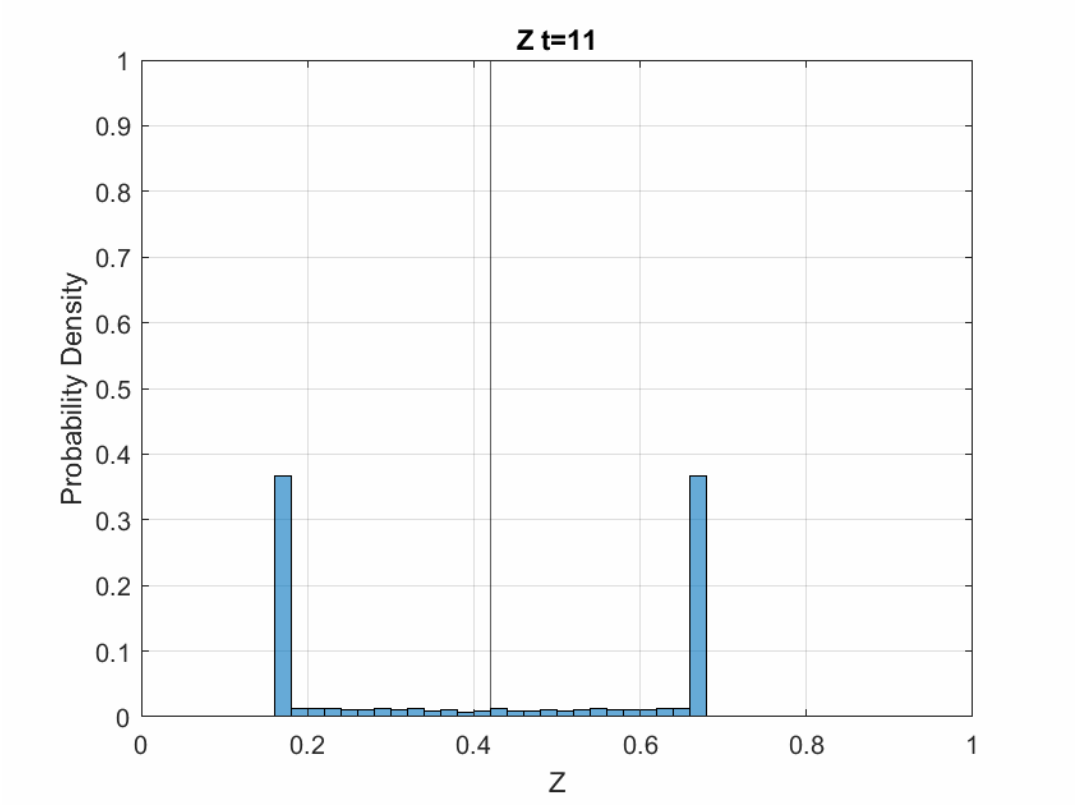
Z t=11
Probability Density
Z
0
0.1
0.2
0.3
0.4
0.5
0.6
0.7
0.8
0.9
1
0.2
0.4
0.6
0.8

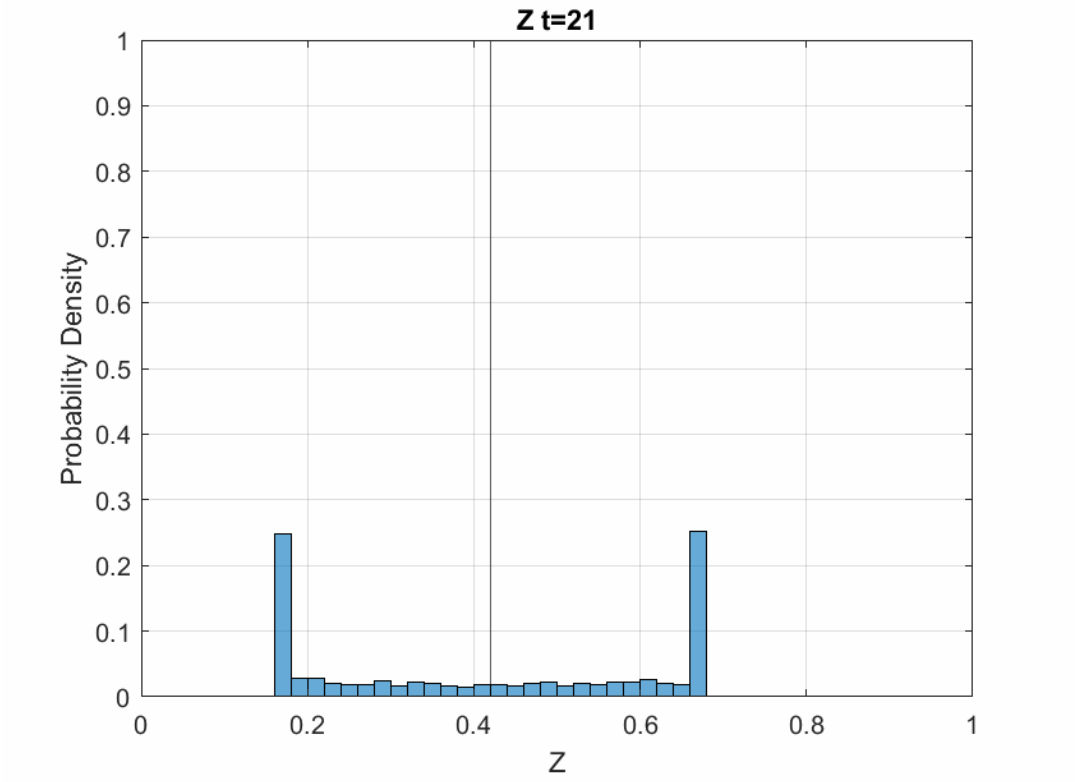
Z t=21
Probability Density
Z
0
0.1
0.2
0.3
0.4
0.5
0.6
0.7
0.8
0.9
1
0.2
0.4
0.6
0.8

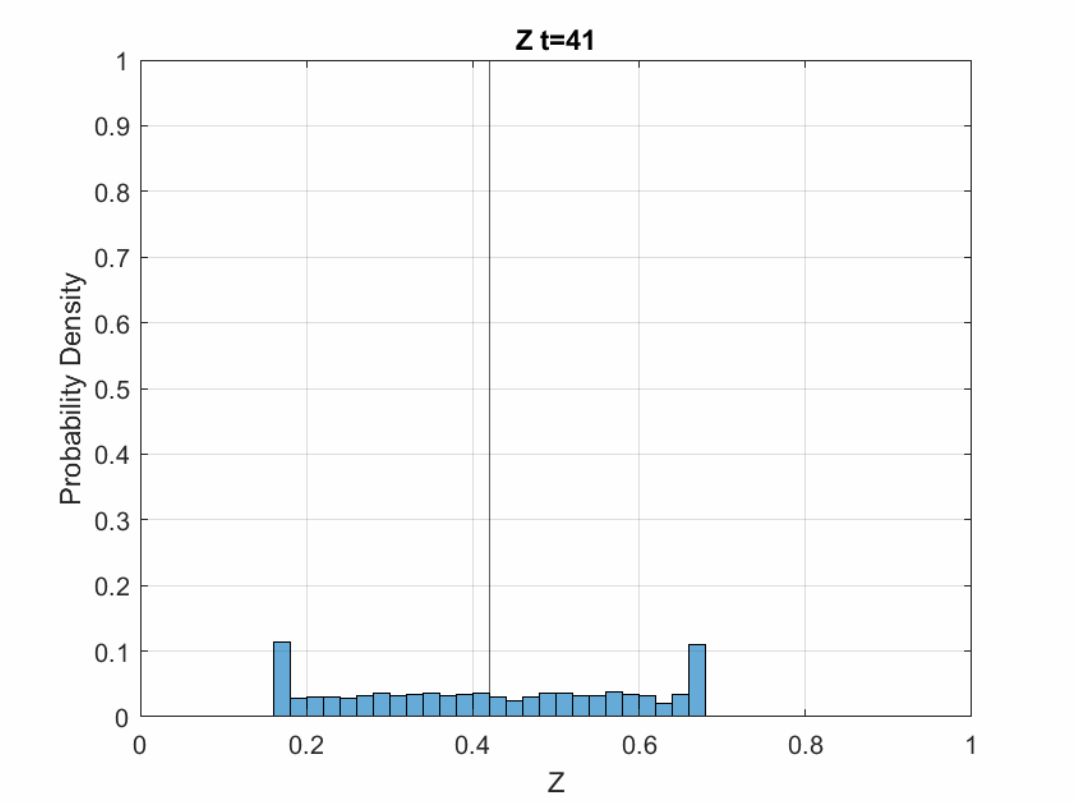
Z t=41
Probability Density
Z
0
0.1
0.2
0.3
0.4
0.5
0.6
0.7
0.8
0.9
1
0.2
0.4
0.6
0.8

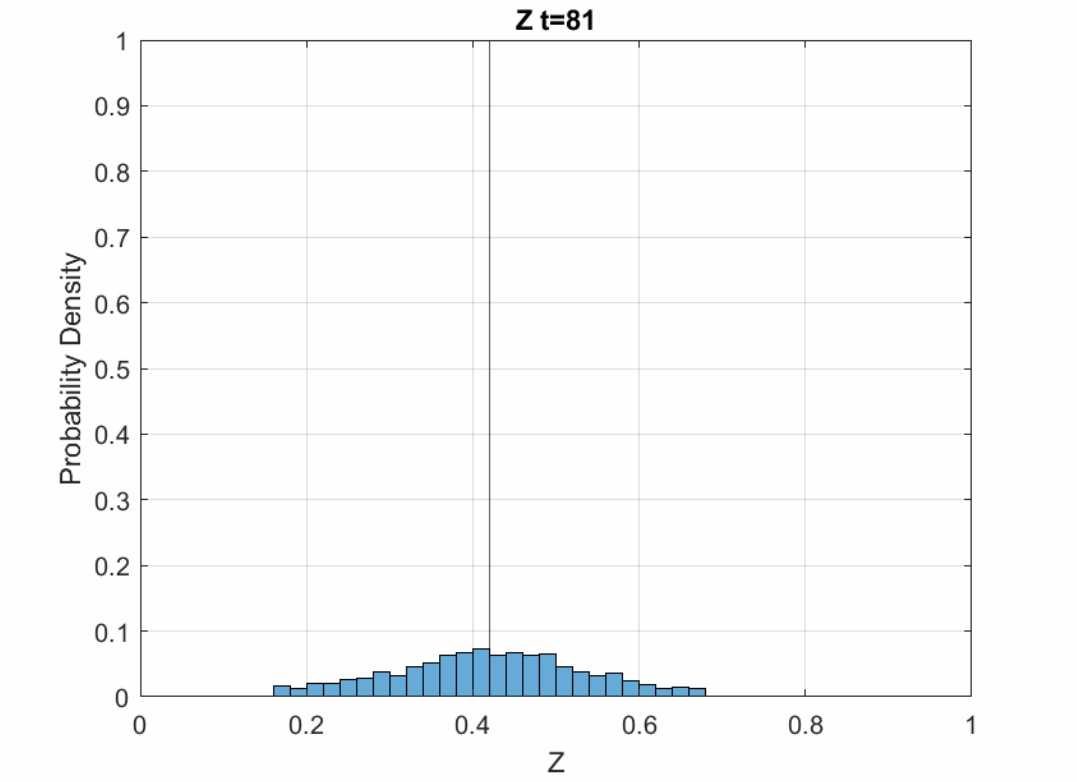
Z t=81
Probability Density
Z
0
0.1
0.2
0.3
0.4
0.5
0.6
0.7
0.8
0.9
1
0.2
0.4
0.6
0.8

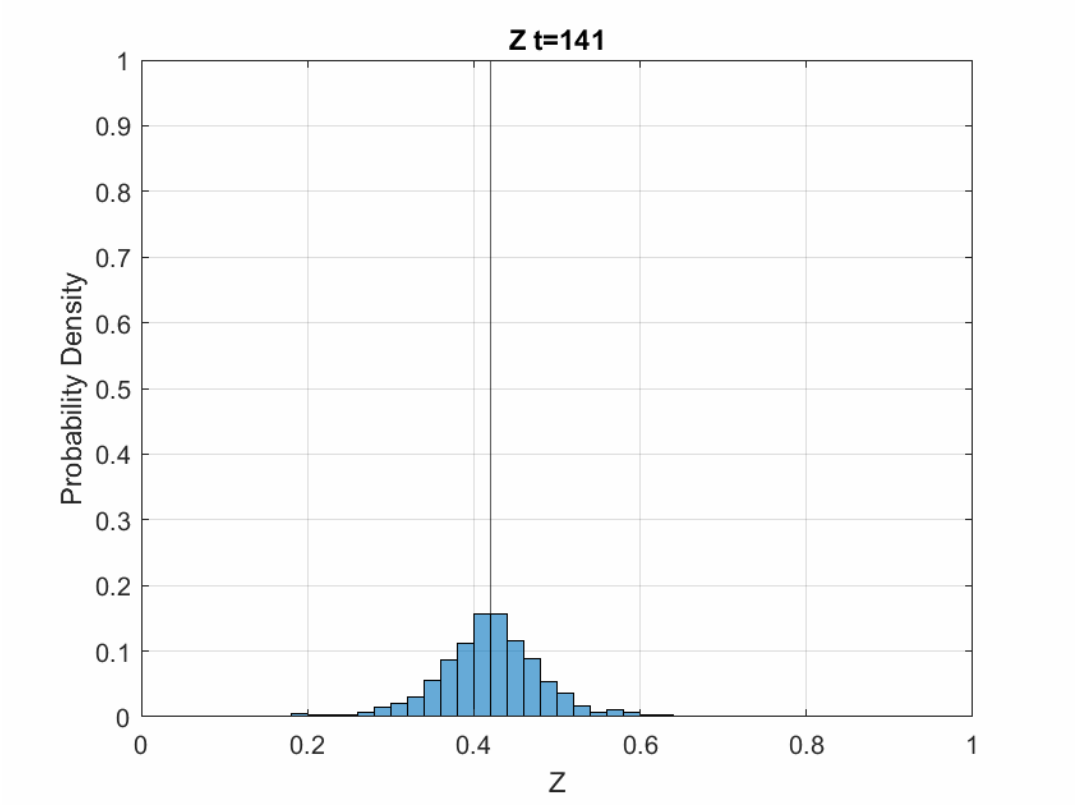
Z t=141
Probability Density
Z
0
0.1
0.2
0.3
0.4
0.5
0.6
0.7
0.8
0.9
1
0.2
0.4
0.6
0.8

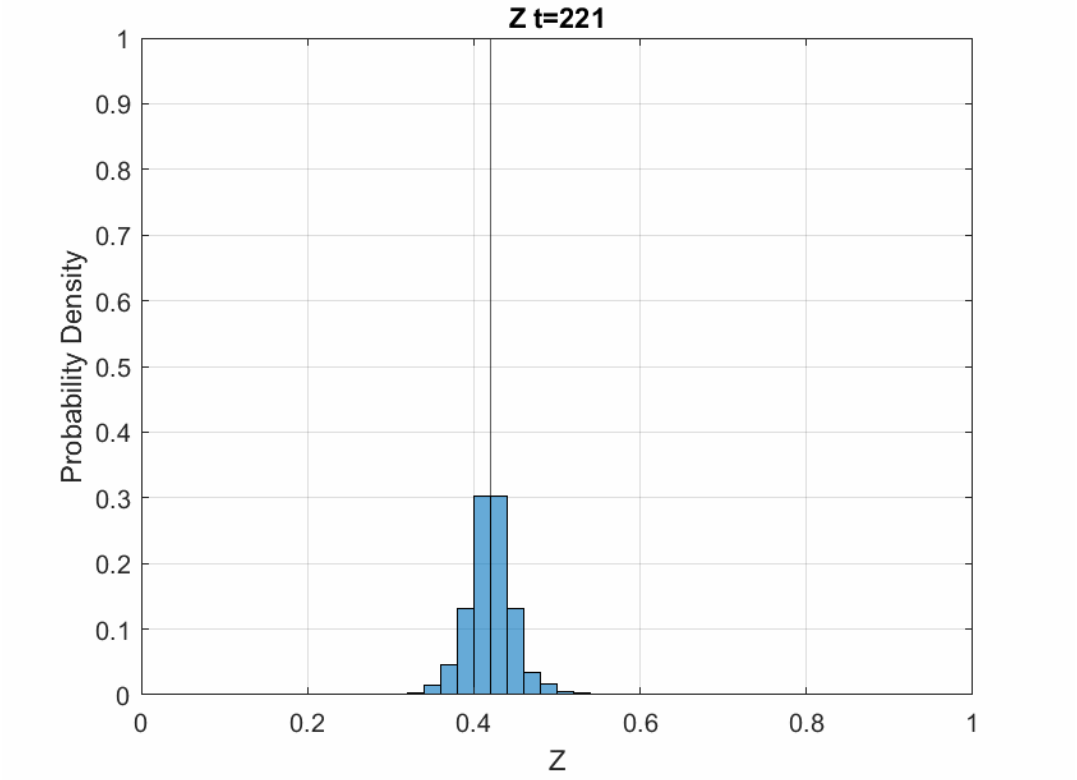
Z t=221
Probability Density
Z
0
0.1
0.2
0.3
0.4
0.5
0.6
0.7
0.8
0.9
1
0.2
0.4
0.6
0.8

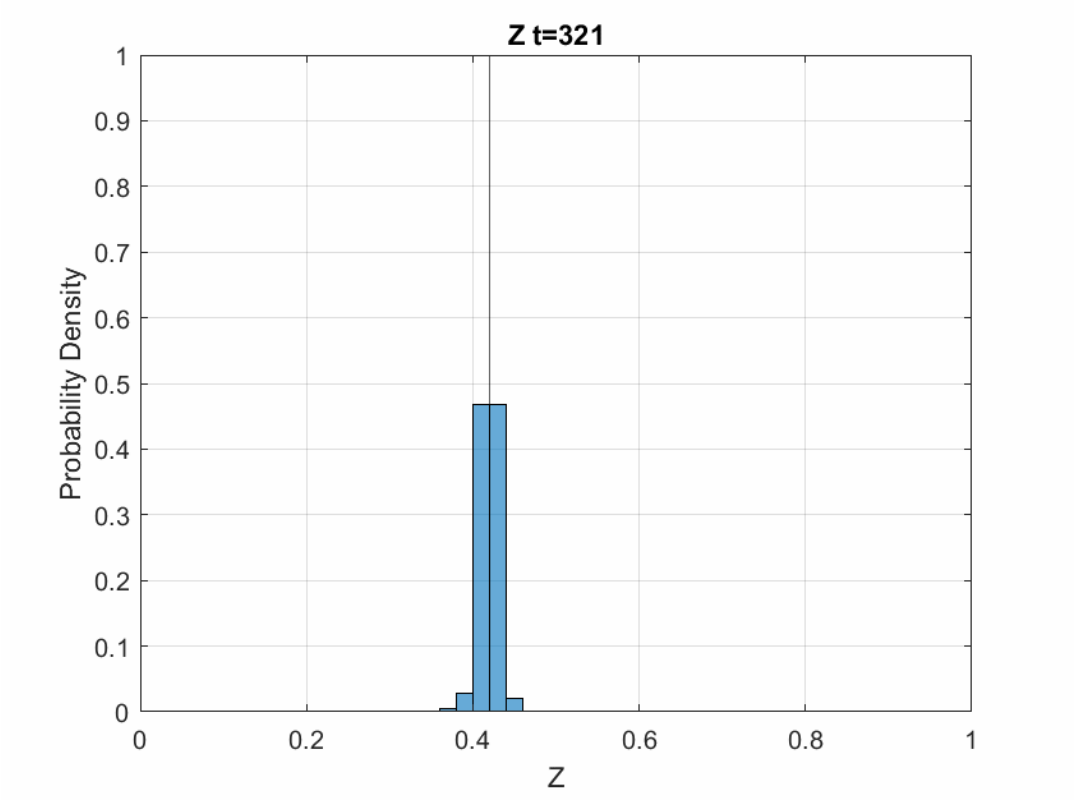

Figure 2.2: Evolution of a PDF using the Coalescence/Dispersion model. The vertical black line indicates the average value.

The same starting conditions as the figures of the IEM model 2.1 have been used. The evolution differs a lot, first it approaches an uniform distribution and after that it converges around the average.

2.3. Mapping Closure model

The third mixing model is called Mapping Closure. [13] In Mapping Closure a Gaussian variable θ is mapped using a time dependent function X onto a field which has the same distribution as the scalar φ. The field $\varphi^s(x,t)$ is the surrogate field $X(\theta,t)$. [10] Since all statistical properties of the Gaussian field θ are known, the statistical properties of φ^s are known too. The goal of this model is to find the function $X(\theta,t)$, where the surrogate field φ^s has some essential properties the same as the original field φ. First the method of mapping a Gaussian function is discussed.

2.3.1. Mapping from a Gaussian

Let φ be a random variable with probability density function (PDF) $f_\varphi(\psi)$ and cumulative density function (CDF) $F_\varphi(\psi)$. Let θ be a Gaussian variable with mean zero and unit variance. The PDF $g_\theta(\eta)$ of θ is

$$g_\theta(\eta) = \frac{1}{\sqrt{2\pi}} \exp\left(-\frac{1}{2}\eta^2\right) \tag{2.9}$$

and the CDF of θ is

$$G_\theta(\eta) \equiv P(\theta < \eta) = \int_{-\infty}^{\eta} \frac{1}{\sqrt{2\pi}} \exp\left(-\frac{1}{2}s^2\right) ds \tag{2.10}$$

The mapping $X(\theta)$ has the same PDF and CDF as φ when

$$P(X(\theta) < \psi) = P(\varphi < \psi) \tag{2.11}$$

A mapping X exists when the CDF $F_\varphi(\psi)$ is a strictly increasing function from 0 to 1. This mapping is unique when X is a nondecreasing function in θ, which leads to

$$G_\theta(\eta) \equiv P(\theta < \eta) = P(X(\theta) < X(\eta)) \tag{2.12}$$

Using (2.11) with $\psi = X(\eta)$

$$P(X(\theta) < X(\eta)) = P(\phi < X(\eta)) \equiv F_\varphi(X(\eta)) \tag{2.13}$$

Hence

$$F_\varphi(X(\eta)) = G_\theta(\eta) \tag{2.14}$$

2.3.2. Three important fields

Mapping Closure uses three different fields.

The first is the turbulent field $\varphi(\vec{x}, t)$. Consider the situation that only the one-point PDF at time t is known. (As is the case in most statistical turbulence models) This is not enough to calculate the PDF at a time $t + \Delta t$, because the statistics of gradients can not be determined. Those gradients are required in this model.

The second is the time-independent Gaussian field $\theta(\vec{x})$. This field is statistically homogeneous and isotropic, which means that all statistics of a field variable is invariant under a shift in position or under a rotation. [7] $\theta(\vec{x})$ is fully determined by the mean, which is taken to be zero. The variance, which is taken to be one and by the spatial two-point correlation function

$$\rho_{cor} \equiv \langle \theta(\vec{x})\theta(\vec{x} + \vec{e}r) \rangle \tag{2.15}$$

where $\vec{e}$ is a random unit vector. This Gaussian field has a associated length-scale given by

$$\lambda_\theta \equiv \left\langle \frac{\partial \theta}{\partial x_i} \frac{\partial \theta}{\partial x_i} \right\rangle^{-\frac{1}{2}} \tag{2.16}$$

Rewriting equation (2.16) gives the expression

$$\left\langle \left(\frac{\partial \theta}{\partial x_i} \right)^2 \right\rangle = \frac{1}{\lambda_\theta^2} \tag{2.17}$$

It can also be deduced that [10]

$$\left\langle \frac{\partial^2 \theta}{\partial x_i^2} \right\rangle = -\frac{\eta}{\lambda_\theta^2} \tag{2.18}$$

The third is a surrogate field $\varphi^s(\vec{x}, t)$. This field is the result of a mapping of the Gaussian field $\theta(\vec{x})$ using the time-dependent function $X(\theta(\vec{x}, t)$. The goal is to construct a field $\varphi^s(\vec{x}, t)$, which has the same distribution as the turbulent field $\varphi(\vec{x}, t)$. Like in equation (2.14) the time-dependent mapping satisfies

$$F_\varphi(X(\eta, t); \vec{x}, t) = G_\theta(\eta; \vec{x}) \tag{2.19}$$

The statistics of the Gaussian field are well known and since the mapping X is known too the surrogate field is known too. For example the derivative of $\varphi^s(\vec{x}, t)$ with respect to x_i using the chain rule is

$$\frac{\partial \varphi^s(\vec{x}, t)}{\partial x_i} = \frac{\partial \theta}{\partial x_i} X^{'}(\theta, t) \tag{2.20}$$

and the second derivative is

$$\frac{\partial^2 \varphi^s(\vec{x}, t)}{\partial x_i^2} = \frac{\partial^2 \theta}{\partial x_i^2} X^{'}(\theta, t) + \left(\frac{\partial \theta}{\partial x_i} \right)^2 X^{''}(\theta, t) \tag{2.21}$$

With

$$X^{'}(\eta, t) = \frac{\partial X(\eta, t)}{\partial \eta} \tag{2.22}$$

and

$$X^{''}(\eta, t) = \frac{\partial^2 X(\eta, t)}{\partial \eta^2} \tag{2.23}$$

Using the definition of the Laplacian and using $\theta(\vec{x}) = \eta$ and $\varphi^s(\vec{x}, t) = X(\eta, t)$ results in

$$\langle \nabla^2 \varphi^s(\vec{x}, t) | \varphi^s(\vec{x}, t) = X(\eta, t) \rangle = \left\langle \frac{\partial^2 \theta}{\partial x_i^2} X^{'}(\theta, t) + \left(\frac{\partial \theta}{\partial x_i} \right)^2 X^{''}(\theta, t) \middle| \theta(\vec{x}) = \eta \right\rangle \tag{2.24}$$

This can be rewritten using equations (2.17) and (2.18) to

$$\langle \nabla^2 \varphi^s(\vec{x},t) | \varphi^s(\vec{x},t) = X(\eta,t) \rangle = \frac{1}{\lambda_\theta^2} \left\{ -\eta X^{'}(\eta,t) + X^{''}(\eta,t) \right\} \tag{2.25}$$

The mapping-closure assumption is as follows:

$$\langle \nabla^2 \varphi(\vec{x},t) | \varphi(\vec{x},t) = \psi \rangle = \langle \nabla^2 \varphi^s(\vec{x},t) | \varphi^s(\vec{x},t) = \psi \rangle \tag{2.26}$$

The unknown statistics of the turbulent field φ is the same as the known statistics of the surrogate field φ^s. The evolution of the PDF is given by [13]

$$\frac{\partial f_\varphi}{\partial t} = -\frac{\partial}{\partial \psi} \left\langle \mathbb{D} \nabla^2 \varphi \middle| \psi \right\rangle f_\varphi \tag{2.27}$$

with diffusion coefficient $\mathbb{D}$. Using the mapping-closure assumption and equation (2.25) results in

$$\frac{\partial f_\varphi(\psi;t)}{\partial t} = -\frac{\partial}{\partial \psi} \left[\mathbb{D} \frac{1}{\lambda_\theta^2} \{ -\eta X^{'}(\eta,t) + X^{''}(\eta,t) \}_{|X(\eta,t)=\psi} f_\varphi(\psi;t) \right] \tag{2.28}$$

This is the full equation for the PDF of the turbulent field.

2.3.3. Time evolution of the mapping

The Gaussian field $\theta(\vec{x})$ does not depend on time, while the PDF of the turbulent field does. That is why the mapping $X(\eta,t)$ does depend on time. Deriving equation (2.19) with respect to time yields

$$\frac{\partial F_\varphi(\psi,t)}{\partial t} + \frac{\partial F_\varphi(X(\eta,t),t)}{\partial \psi} \frac{\partial X(\eta,t)}{\partial t} = 0 \tag{2.29}$$

The evolution of the distribution F_φ using equation (2.27) is

$$\frac{\partial F_\varphi(\psi,t)}{\partial t} + \frac{\partial F_\varphi(\psi,t)}{\partial \psi} \mathbb{D} \left\langle \nabla^2 \varphi \middle| \varphi(\vec{x},t) = \psi \right\rangle = 0 \tag{2.30}$$

Combining the last two equations with $\psi = X(\eta,t)$ gives an equation for the time evolution of the mapping

$$\frac{\partial X(\eta,t)}{\partial t} = \mathbb{D} \left\langle \nabla^2 \varphi \middle| \varphi(\vec{x},t) = X(\eta,t) \right\rangle \tag{2.31}$$

By using the mapping-closure assumption and equation 2.25 the evolution becomes

$$\frac{\partial X(\eta,t)}{\partial t} = \frac{\mathbb{D}}{\lambda_\theta^2} \left\{ -\eta X^{'}(\eta,t) + X^{''}(\eta,t) \right\} \tag{2.32}$$

Instead of $\frac{\mathbb{D}}{\lambda_\theta^2}$, the mixing frequency ω_X could also be used.

2.3.4. Particle method

Just like the IEM model and the CoDi model, MC can also be solved using particles. First a sketch of the CDF's $G_\theta(\eta)$ and $F_\varphi(\psi)$ is shown to indicate the definitions of η and ψ for the particle method.

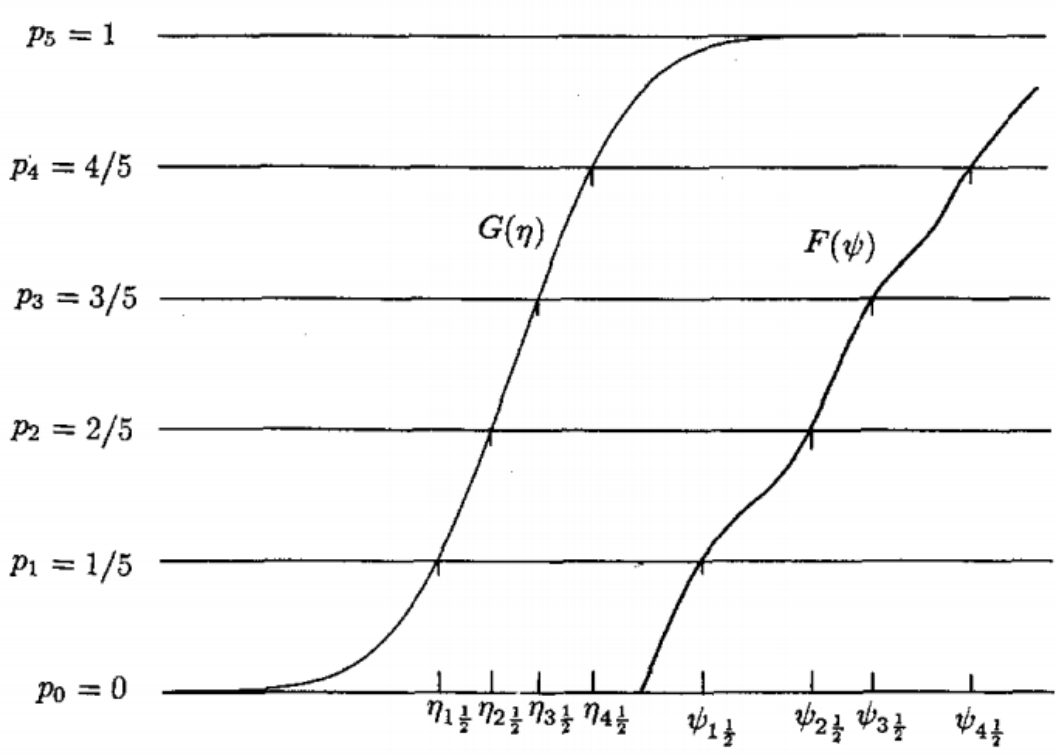

Figure 2.3: Sketch of CDF's $G_\theta(\eta)$ and $F_\varphi(\psi)$ showing the definitions of $\eta_{i+1/2}$ and $\psi_{i+1/2}$ for 5 particles. [10]

For 5 particles $N = 5$ the interval $[0,1]$ is split into 5 parts. The horizontal lines are the probabilities

$$p_i \equiv \frac{i}{N} \qquad i = 0,1,...,N \tag{2.33}$$

$G_\theta(\eta)$ is the CDF of the Gaussian θ and $F_\varphi(\psi)$ is the CDF corresponding to the turbulent field φ. $\eta_{i+1/2}$ belongs to the point where the CDF $G_\theta(\eta)$ is equal to p_i. And similarly $\psi_{i+1/2}$ belongs to the point where the CDF $F_\varphi(\psi)$ is equal to p_i. The scalar of particle i is defined by as $\varphi_i(t)$ with $\psi_{i-1/2} \leq \varphi_i(t) \leq \psi_{i+1/2}$. Note that this collection of particles $\varphi_i(t)$ is ordered with φ_1 the lowest and φ_N the highest. The actual value of $\varphi_i(t)$ is approximated by the mean value on the interval $[\psi_{i-1/2}, \psi_{i+1/2}]$.

$$\varphi_i(t) \equiv \frac{\int_{\psi_{i-1/2}}^{\psi_{i+1/2}} \psi f_\varphi(\psi;t)d\psi}{\int_{\psi_{i-1/2}}^{\psi_{i+1/2}} f_\varphi(\psi;t)d\psi} \tag{2.34}$$

The integral in the denominator is calculated by integrating.

$$\int_{\psi_{i-1/2}}^{\psi_{i+1/2}} f_\varphi(\psi;t)d\psi = F_\varphi(\psi_{i+1/2}) - F_\varphi(\psi_{i-1/2}) = p_i - p_{i-1} = \frac{i}{N} - \frac{i-1}{N} = \frac{1}{N} \tag{2.35}$$

When using $\psi = \varphi = X(\eta,t)$, $f_\varphi(\psi;t)$ becomes $g_\theta(\eta)$, so

$$\varphi_i(t) = N\int_{\eta_{i-1/2}}^{\eta_{i+1/2}} X(\eta,t)g_\theta(\eta)d\eta \tag{2.36}$$

Differentiating equation (2.36) gives the evolution of φ_i over time. η does not depend on time so the differentiation can be taken inside the integral.

$$\frac{d\varphi_i(t)}{dt} = N\int_{\eta_{i-1/2}}^{\eta_{i+1/2}} \frac{\partial X(\eta,t)}{\partial t} g_\theta(\eta)d\eta \tag{2.37}$$

Substituting $\frac{\partial X(\eta,t)}{\partial t}$ using equation (2.32) to obtain

$$\frac{d\varphi_i(t)}{dt} = \frac{\mathbb{D}N}{\lambda_\theta^2}\int_{\eta_{i-1/2}}^{\eta_{i+1/2}} \left\{-\eta X^{'}(\eta,t) + X^{''}(\eta,t)\right\} g_\theta(\eta)d\eta \tag{2.38}$$

The derivative of $g_\theta(\eta)$ can be easily calculated.

$$\frac{dg_\theta(\eta)}{d\eta} = -\eta g_\theta(\eta) \tag{2.39}$$

With this information the part inside the integral can be seen as a derivative of $g_\theta(\eta)X^{'}(\eta,t)$ with respect to η. Now the evolution of $\varphi_i(t)$ becomes

$$\frac{d\varphi_i(t)}{dt} = \frac{\mathbb{D}N}{\lambda_\theta^2}\int_{\eta_{i-1/2}}^{\eta_{i+1/2}} \frac{\partial}{\partial\eta}\left\{g_\theta(\eta)X^{'}(\eta,t)\right\}d\eta = \frac{\mathbb{D}N}{\lambda_\theta^2}\left[g_\theta(\eta)X^{'}(\eta,t)\right]_{\eta_{i-1/2}}^{\eta_{i+1/2}} \tag{2.40}$$

$X^{'}(\eta,t) = \frac{\partial X(\eta,t)}{\partial\eta}$ needs to be calculated at $\eta = \eta_{i+1/2}$ and $\eta = \eta_{i-1/2}$. The differentiation is approximated by the central difference formula $\frac{X(\eta+h,t)-X(\eta-h,t)}{2h}$. The center is taken at $\eta_{i+1/2}$ with h such that $\eta_{i+1/2}+h = \eta_{i+1}$ and $\eta_{i+1/2}-h = \eta_i$. Now

$$\frac{\partial X(\eta_{i+1/2},t)}{\partial\eta} \approx \frac{X(\eta_{i+1},t)-X(\eta_i,t)}{\eta_{i+1}-\eta_i} \tag{2.41}$$

$X(\eta,t)$ is substituted back for φ resulting in the full equation for the evolution of particle i with φ_i depending on itself and on the values of φ close to φ_i.

$$\frac{d\varphi_i(t)}{dt} = (\varphi_{i+1}(t)-\varphi_i(t))B_{i+1/2} - (\varphi_i(t)-\varphi_{i-1}(t))B_{i-1/2} \tag{2.42}$$

where

$$B_{i+1/2} \equiv \frac{\mathbb{D}N}{\lambda_\theta^2}\frac{g_\theta(\eta_{i+1/2})}{\eta_{i+1}-\eta_i} \tag{2.43}$$

The particles φ_1 and φ_N can not use the values of particles above and below itself, because they are already the lowest/highest. That is why for those particles the evolutions become

$$\frac{d\varphi_1(t)}{dt} = (\varphi_2(t)-\varphi_1(t))B_{3/2} \tag{2.44}$$

and

$$\frac{d\varphi_N(t)}{dt} = -(\varphi_N(t)-\varphi_{N-1}(t))B_{N-1/2} \tag{2.45}$$

with the same definition of B. This is a system of differential equations which can be solved numerically.

In these differential equations, the scalars φ change with an amount proportional to differences in composition compared to particles with similar composition. That is why unlike in IEM or CoDi the evolution of mixing will have peaks that slowly branch off. In CoDi the peaks would decrease but the particles coming from those peaks were uniformly distributed between two starting peaks. In MC these particles stay close to the initial peaks.

In the figures below distributions at different moments in time are shown. Mixing is done using MC. Z is a scalar which belongs to the particles getting mixed.

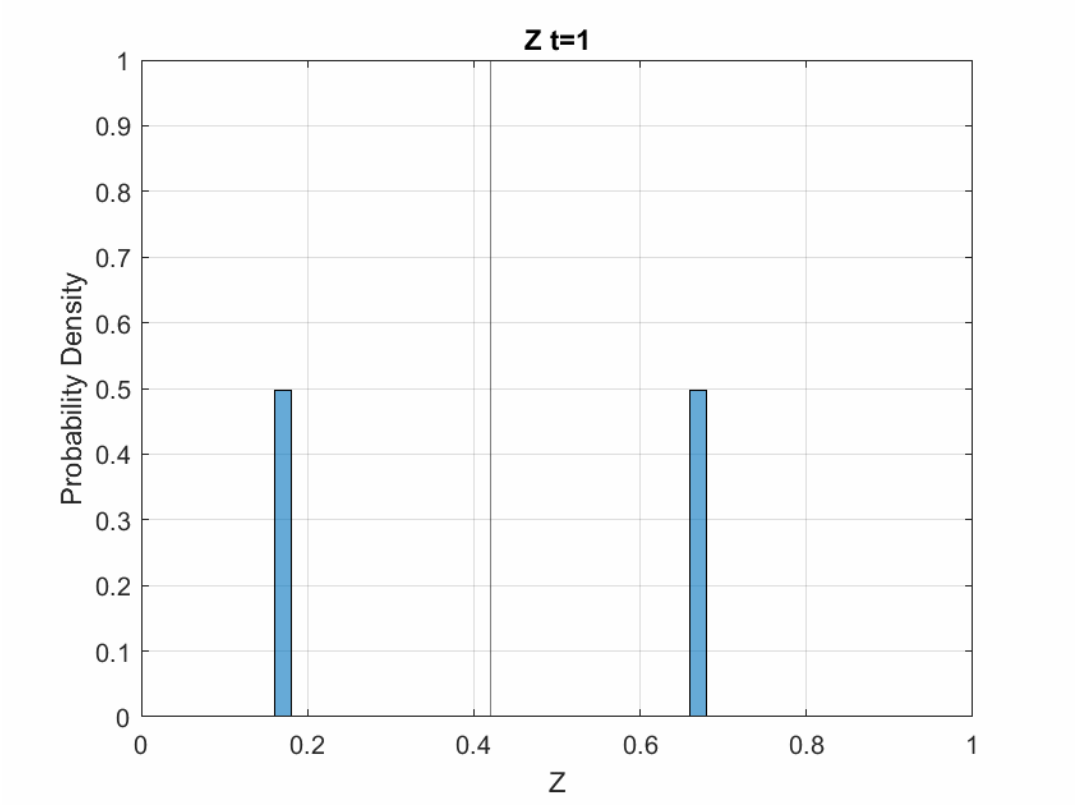
Z t=1
Probability Density
Z
0
0.1
0.2
0.3
0.4
0.5
0.6
0.7
0.8
0.9
1
0.2
0.4
0.6
0.8

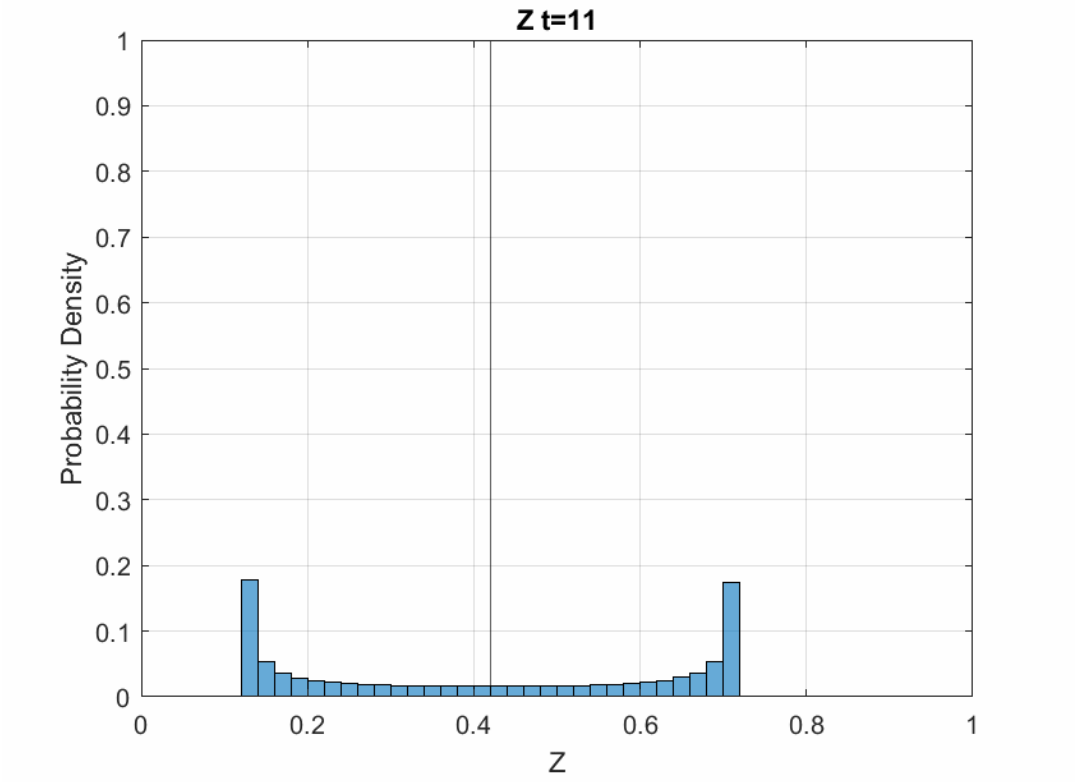
Z t=11
Probability Density
Z
0
0.1
0.2
0.3
0.4
0.5
0.6
0.7
0.8
0.9
1
0.2
0.4
0.6
0.8

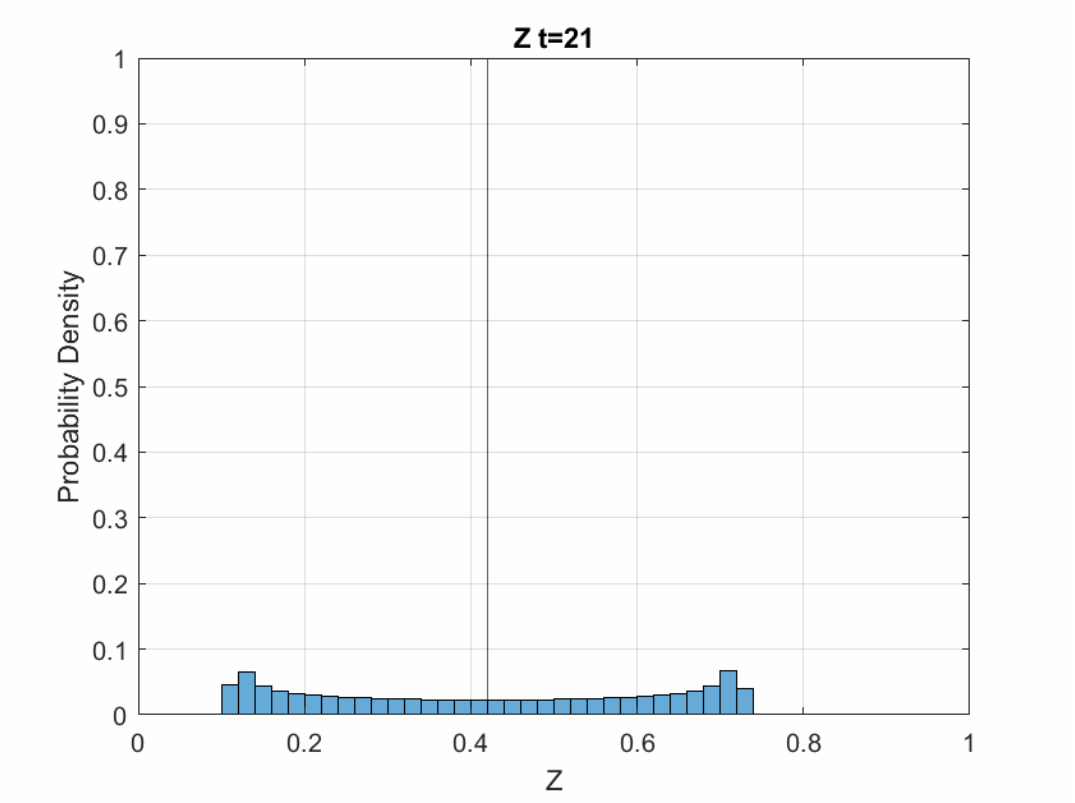
Z t=21
Probability Density
Z
0
0.1
0.2
0.3
0.4
0.5
0.6
0.7
0.8
0.9
1
0.2
0.4
0.6
0.8

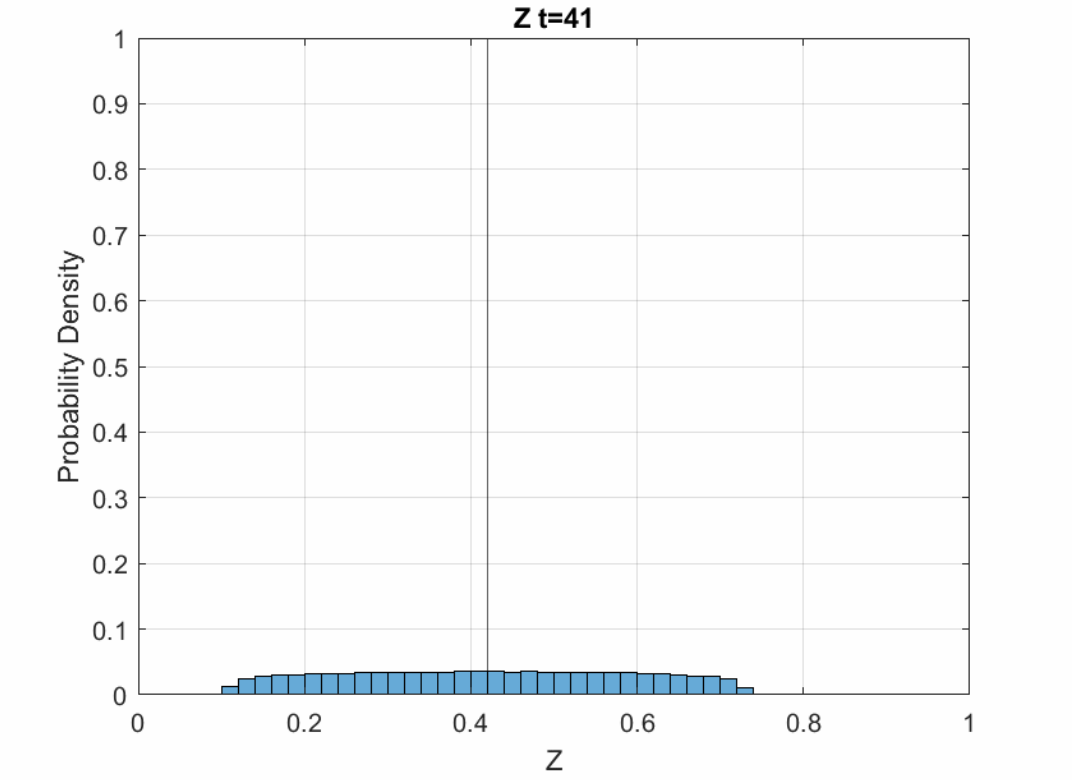
Z t=41
Probability Density
Z
0
0.1
0.2
0.3
0.4
0.5
0.6
0.7
0.8
0.9
1
0.2
0.4
0.6
0.8

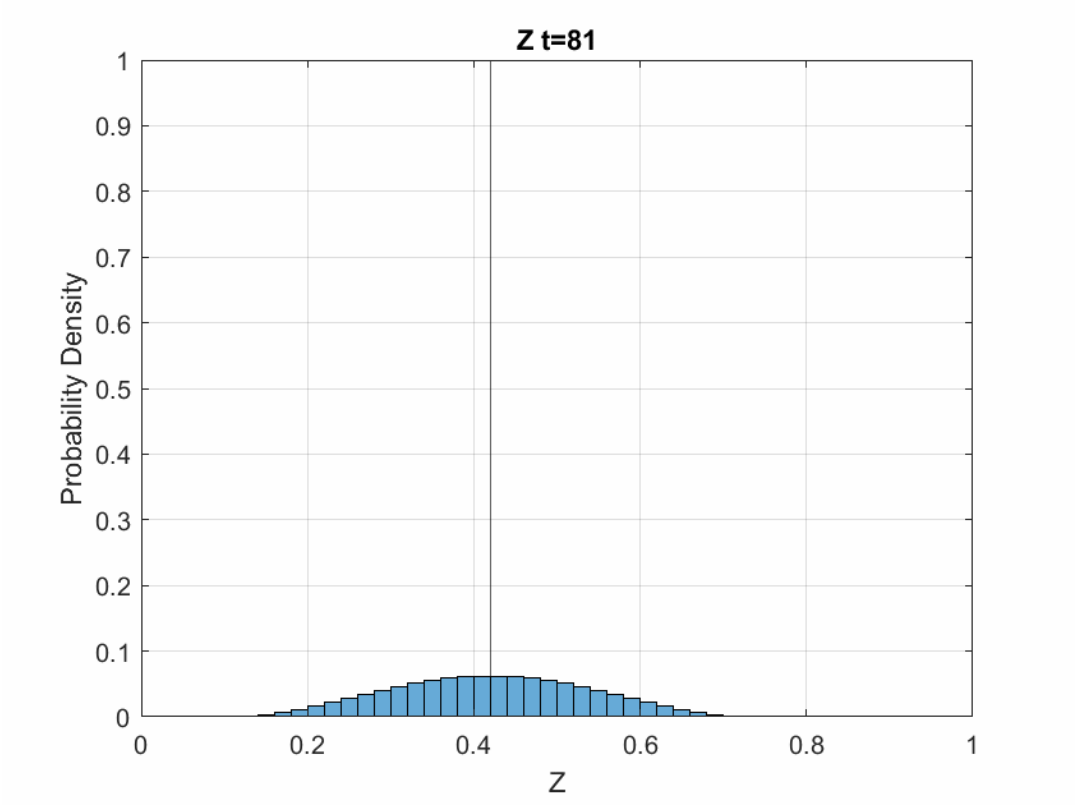
Z t=81
Probability Density
Z
0
0.1
0.2
0.3
0.4
0.5
0.6
0.7
0.8
0.9
1
0.2
0.4
0.6
0.8

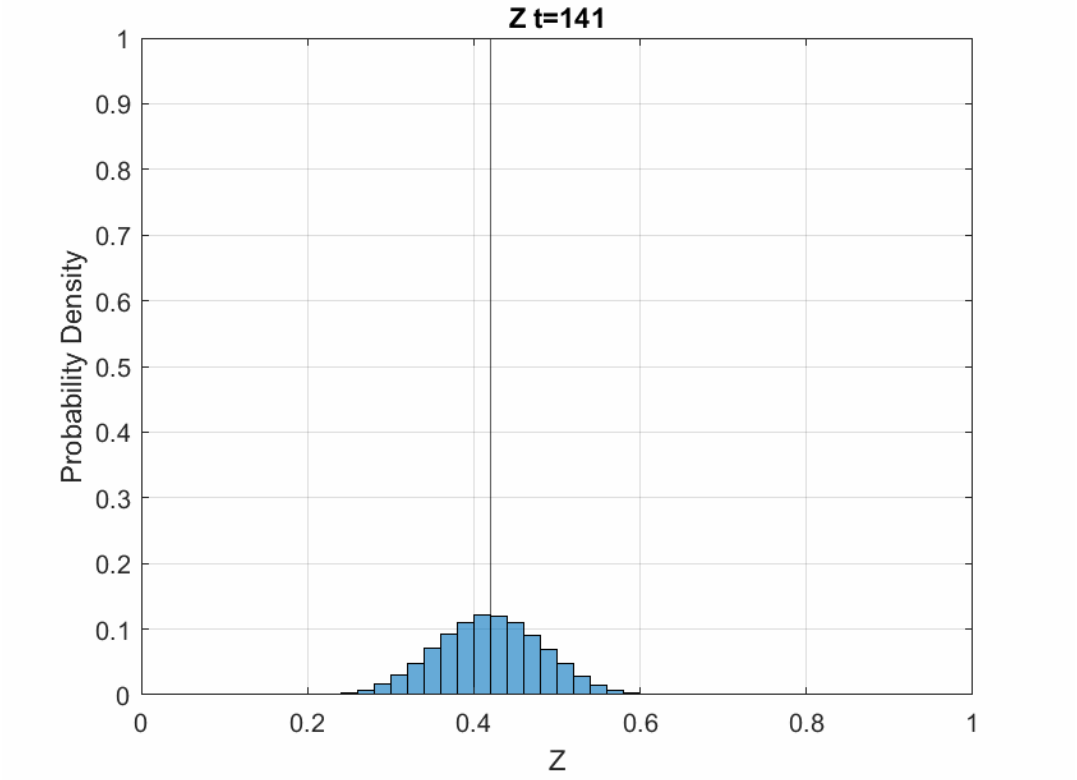
Z t=141
Probability Density
Z
0
0.1
0.2
0.3
0.4
0.5
0.6
0.7
0.8
0.9
1
0.2
0.4
0.6
0.8

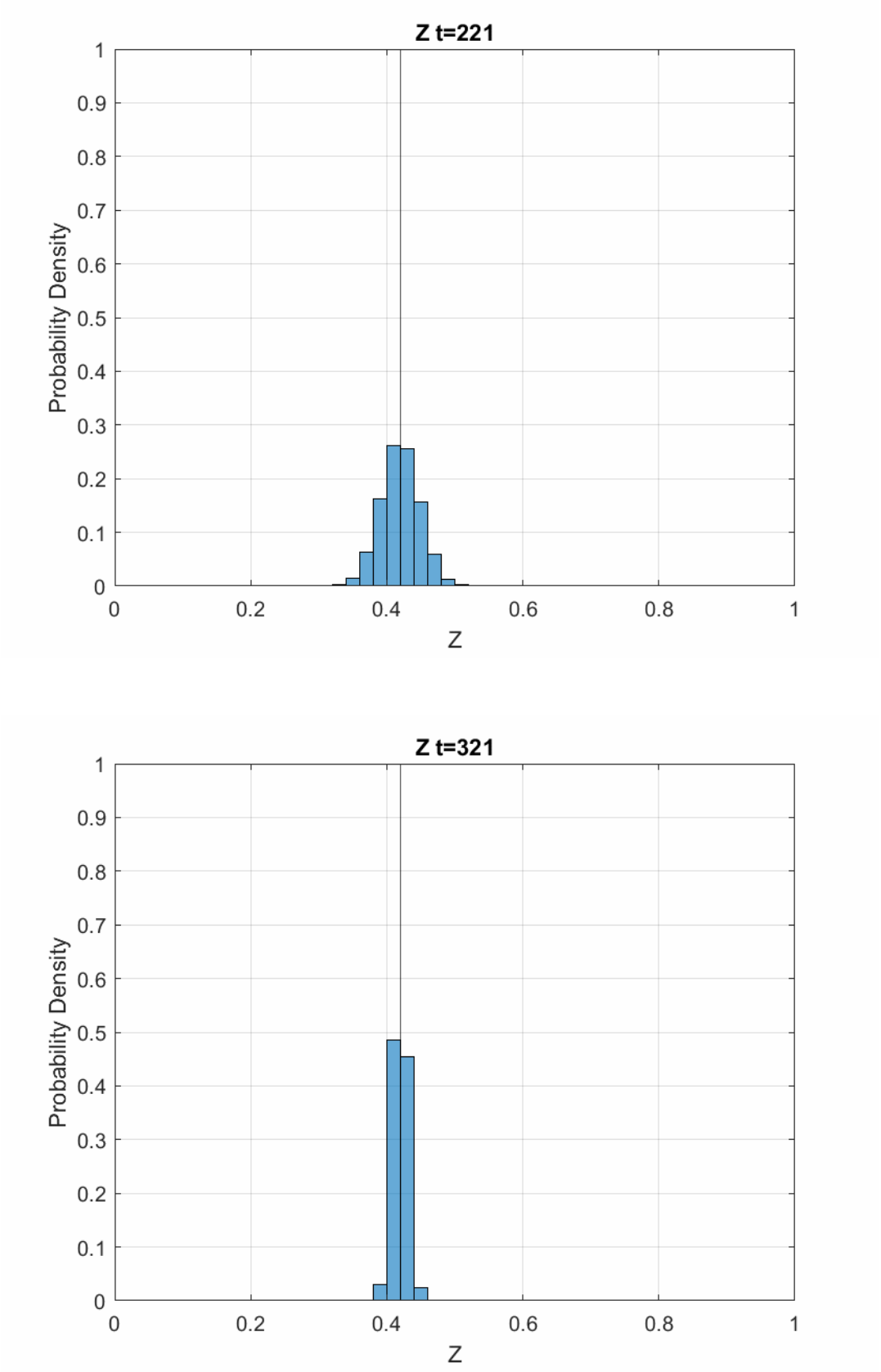

Figure 2.4: Evolution of a PDF using the Mapping Closure model. The vertical black line indicates the average value.

Again the same starting condition as usual for IEM and CoDi has been used in these figures. It may look

similar to the figures of CoDi, but there are some important differences. In MC the particles take the particles with values close to itself into account. That is why, in the first steps, the values still stay close to the initial values, while in CoDi the values got distributed uniformly between the peaks. Later the PDF converges to a Gaussian around the average.

2.4. Differences in mixing models

Three different micromixing models have been discussed and there are many more. For example the Langevin model. These other micromixing models are beyond the scope of this article, so only IEM, CoDi and MC will be analysed.

IEM and CoDi are used most often because they are easy to extend when there are multiple independent scalars. They are also easy to implement. A disadvantage of both models is their physical representation. They do converge to the right value but their evolution in time differs a lot from the Navier-Stokes equations. MC however is much better in agreement with the Navier-Stokes equations. [16] In general MC can not be generalised to more than one independent scalar.

The difference in predictions from the three models will be investigated in the case of supercritical water.

3 Program

3.1. MM-INTAS

All three mixing models discussed in chapter 2 are implemented in a program called MM-INTAS. [9] It is written in the Fortran language. MM-INTAS is able to run simulations of mixing. The program runs in three sections. They are the initialisation, the mainloop and the exit section. In the initialisation section, the input about how many particles, kind of starting distribution and mixing method is read into the program. This information is used to generate a starting distribution, where each particle has its own properties. The mainloop section is about the development over time. On one time step multiple actions take place. These actions are mixing, looking up the new dependent properties and writing an output file. An algorithm where multiple actions take place on the same time step is called a time splitting algorithm. At the exit section the opened files are closed and the program is ended. A detailed schematic of MM-INTAS is shown in figure 3.1

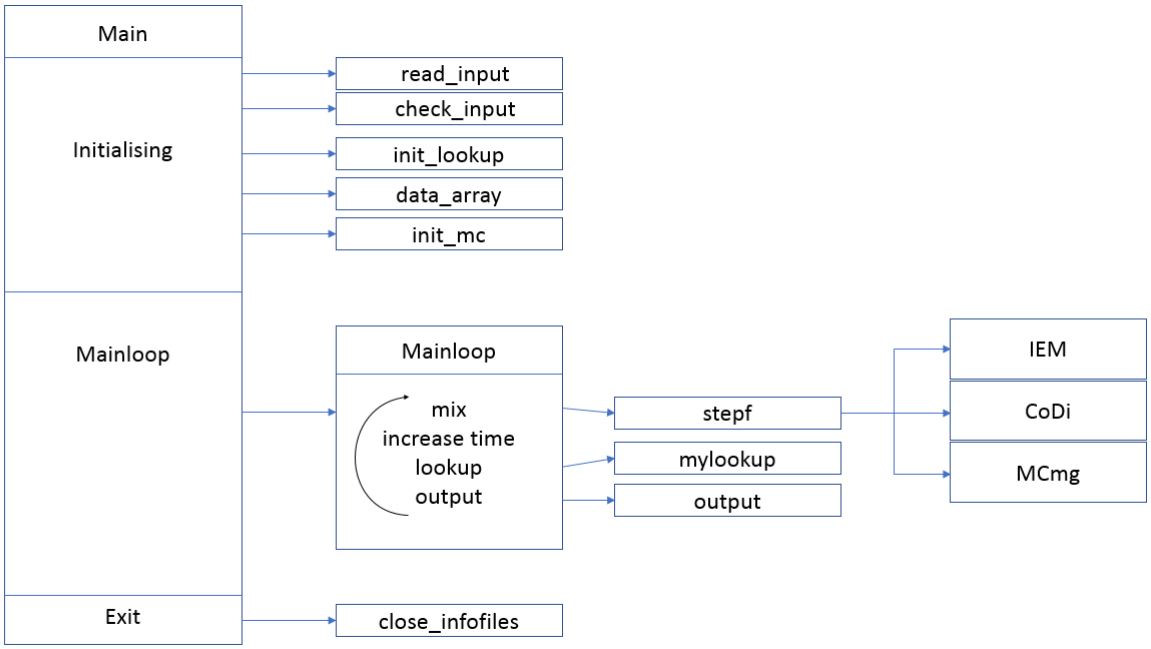

Figure 3.1: An overview of the different parts of MM-INTAS. On the left is the main file with the three sections. An arrow pointing to the right means that the file on the left is calling the file or function on the right. The curved arrow indicates a loop meaning that the steps inside get repeated a certain amount of times.

Check_input makes sure that the input given by read_input is accepted by the program. Data_array generates the lookup table which is used in the lookup function. The function stepf can choose between the three

mixing models IEM, CoDi and MC. The choice of mixing method is given in the input files and used in stepf to call the function corresponding to the mix method. Mylookup uses linear interpolation and the lookup table to find the values of the other properties. Output generates text files of the properties of every particle in one big table. These data files can be used to analyse the results, how this is done is discussed in 3.3 That is everything about the structure of MM-INTAS.

Compiling a Fortran program which uses multiple files can be quite difficult. A few tips about how to compile a Fortran program is written in the appendix A.2.

3.2. Choice of independent variable

There are two types of variables used, independent variables and dependent variables. In MM-INTAS, only one independent variable is used. The independent variable is the only property of the system which is determined by the mixing process. All other variables, which are called the dependent variables, are determined using the new value of the independent variable. The mean of the independent variable stays constant over time. As seen in 1.2 all properties are plotted as dependencies on temperature. The temperature however should not necessary stay constant during mixing, so temperature should not be taken as independent variable. The specific enthalpy is better suited. At constant pressure the change in enthalpy depends only on external heat transfer. Assuming this mixing process is closed off from external factors, the enthalpy stays constant. This means that at every mixing step the expected value of the enthalpy should stay constant. To make sure this is the case, the specific enthalpy is taken as the independent variable. Since the specific enthalpy as function of temperature was strictly monotone and located on a closed interval, this function can be inverted. This inverse function makes sure that the values of specific enthalpy have a corresponding temperature. This temperature can then be used to determine all other properties. This last step is not needed in the program, because a table is used which contains specific enthalpy, temperature and the other dependent variables.

3.3. Postprocessing

MM-INTAS is able to generate text files with the values of the properties of the particles. The results are analysed in a different program using MATLAB [1]. First the amount of time steps is checked by looking for all file names containing the same content in the title. For example the file names of "test1" are all of the format "test1_[x]" where [x] is the specified time step. After that a for loop is used to gather all data from the text files. That data is then used to either plot the PDF or plot averages of certain properties over time.

4

Results & Discussion

4.1. Results

A important property of the system is the average temperature. It shows if a flame would spontaneously ignite or if a flame would extinct. Simulations are used in order to see if the different mixing models have the same average temperature over time. The average temperature for the three mixing models is shown in figure 4.1. All models use the same starting conditions. In this case the initial temperatures are below T_c. The mean turbulence frequency $\omega = 100s^{-1}$, the mix model constant $c = 2$. MM-INTAS used time steps of $1 \cdot 10^{-4}$ s and the total number of steps is 400. 2000 particles are used in all simulations. The program only outputs a text file every 10th step, so every time step in the figures mean 10 time steps in the program.

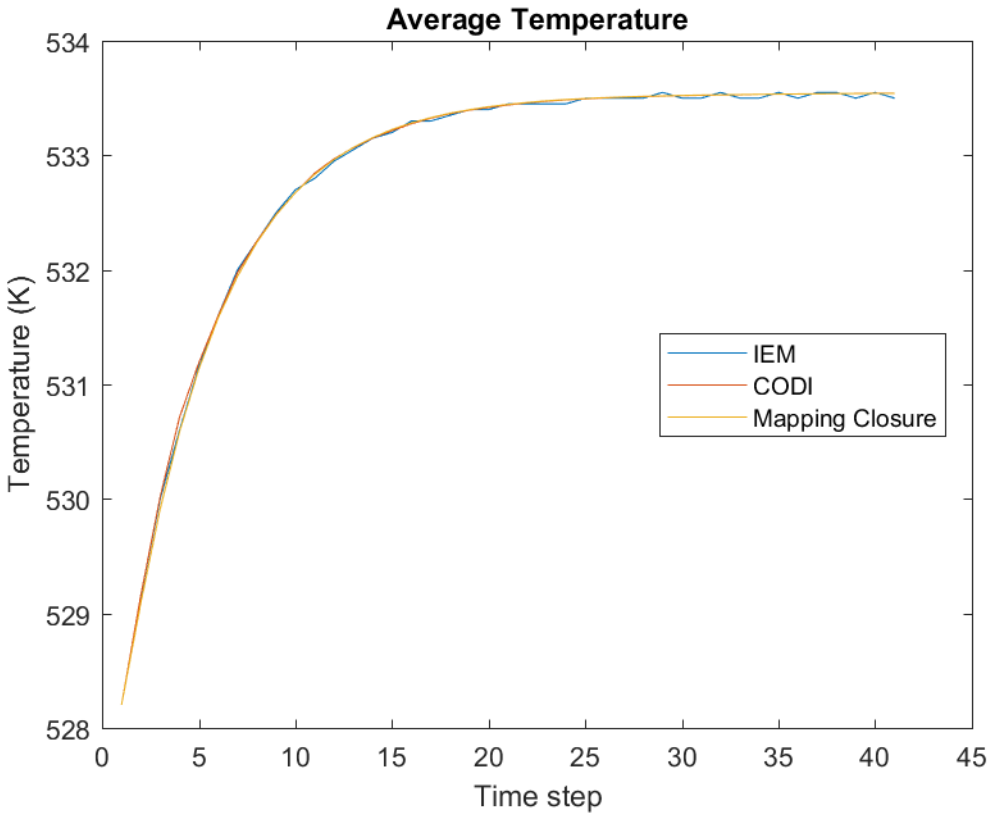

Figure 4.1: The average temperature over time using the mixing models IEM, CoDi and MC. The starting conditions are two equal peaks with temperatures 453.16 K and 603.16 K. Both are below the critical temperature.

All three mixing models give the same average temperature over time. Another interesting remark is that

the average temperature only changed about 5 K, which is much smaller than the difference in starting temperatures which is 150 K. The fact that the mean temperature changes while the mean enthalpy remains constant, is due to the fact that the specific heat capacity depends in a nonlinear way on the temperature. (See figure 1.3)

In the next case every constant is the same as previous case. The only difference is the starting temperatures. They are 753.16 K and 903.16 K, which are both above the critical temperature. Figure 4.2 shows the results of this simulation.

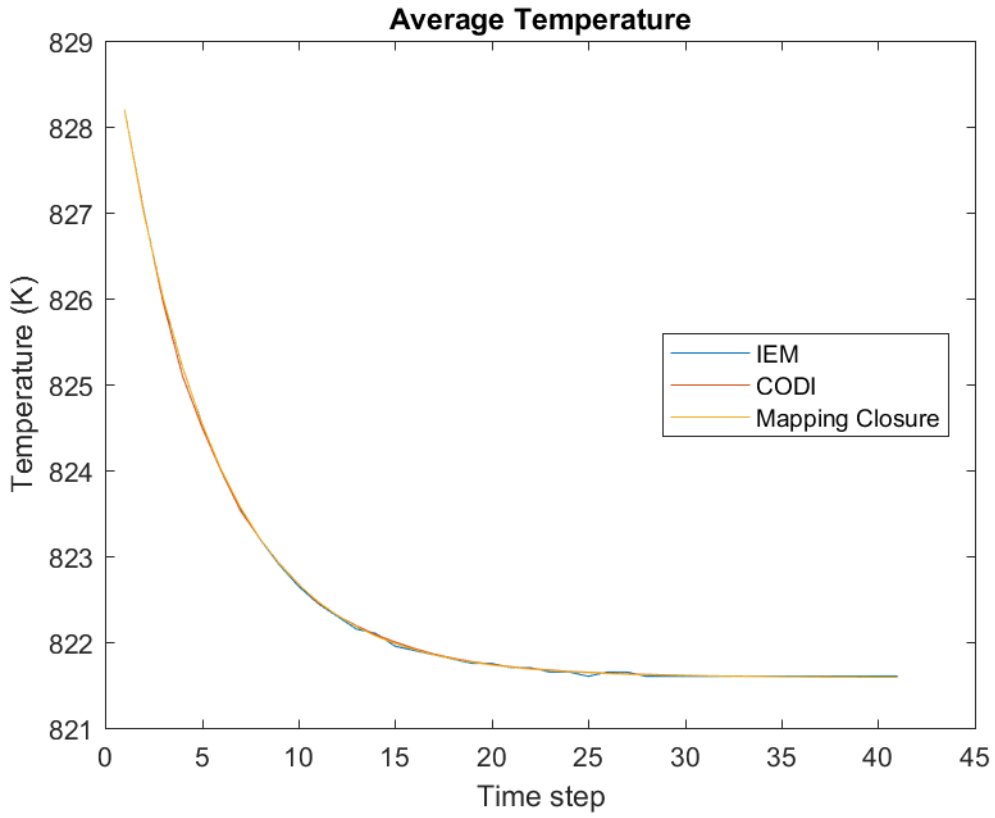

Figure 4.2: The average temperature over time using the mixing models IEM, CoDi and MC. The starting conditions are two equal peaks with temperatures 753.16 K and 903.16 K. Both are above the critical temperature.

Again all three mixing models give the same results in average temperature. Also the difference in average temperature is about 8 K.

The next case however shows a big difference in the mixing models. To make this better visible the amount of time steps is multiplied by 10 (so now it is 4000) while the time step is divided by 10 to make sure the same time interval is used. The amount of particles, ω and c all stayed the same. Now the starting temperatures of the peaks are above and below the critical temperature. These are 453.16 K and 753.16 K. The results are shown in figure 4.3

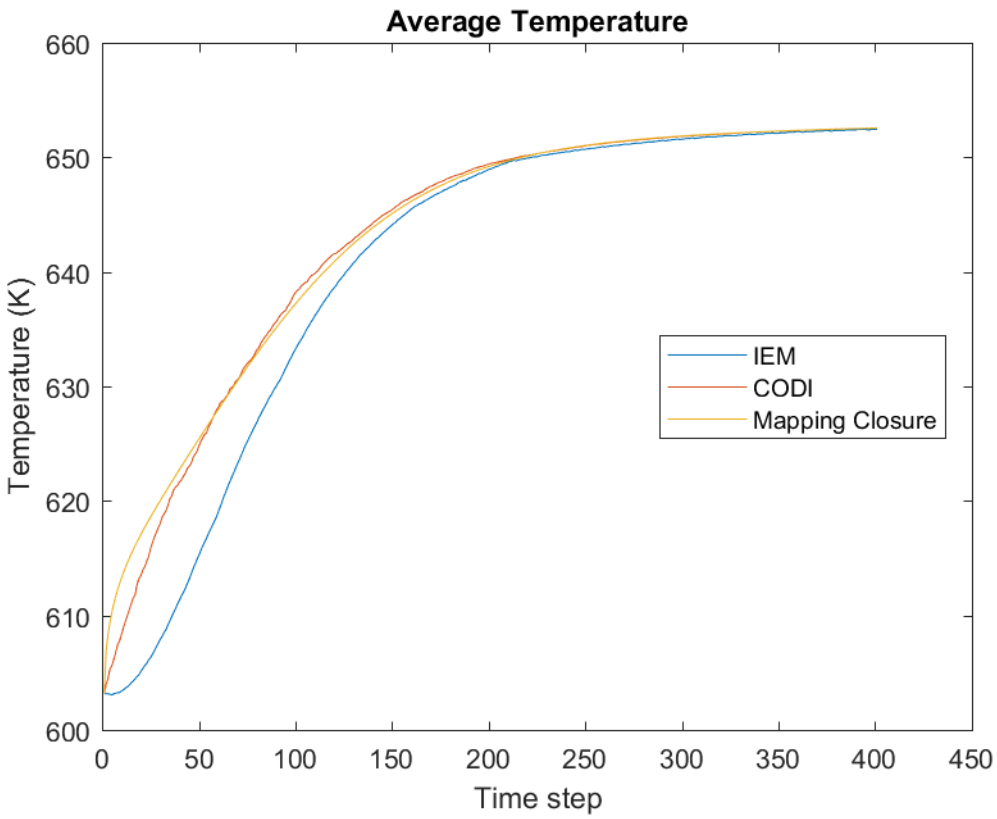

Figure 4.3: The average temperature over time using the mixing models IEM, CoDi and MC. The starting conditions are two equal peaks with temperatures 453.16 K and 753.16 K. The first is below and the second is above the critical temperature.

At the first steps the three mixing models all give a different value for the average temperature. After a short time however CoDi gives the same results as the Mapping Closure model. IEM deviates a lot from the other models. Explanations for this behaviour is given in 4.2. After a long time all three models give the same average temperature again. Comparing this to figures 4.1 and 4.2 seems to indicate that the mixing occurs slower, because it takes a longer time for the average temperature to converge. The reason for this is that the difference in starting temperatures is 300 K compared to 150 K of the other cases. Something that is really different from the first two cases is the difference in average temperature. The difference is about 45 K, on a scale of 300 K this is still a lot higher than 8 K on 150 K. This is also discussed in section 4.2.

4.2. Discussion

Figure 4.3 showed that using IEM resulted in a different average temperature, but that in the end it was the same as the other models. The fact that in the limit all mixing models give the same average is a necessary condition of mixing following from energy conservation. In mixing the average of the independent variable should stay constant, this is the case and shown in figure 4.4. Since the distribution always converges to the average all mixing models converge to a distribution around the same average. In the limit this is one sharply peaked distribution or a sharply peaked distribution still containing the shape of the initial condition in the case of IEM. Obviously these distributions are located at the average meaning that the average in the limit is the same for every mixing model. That is why all three models give the same average temperature at the end.

At intermediate times the models can give different values for the mean temperature, because they lead to different mixing scenarios with different intermediate states. All intermediate states of all three models have the same total enthalpy, but a different temperature distribution over particles.

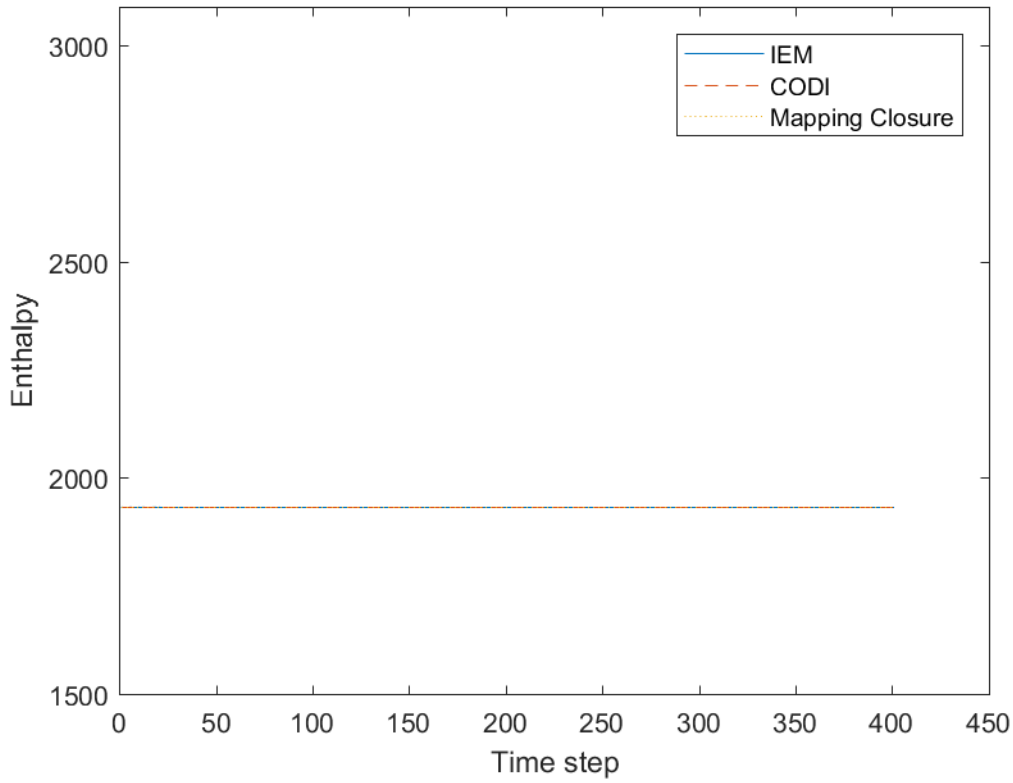

Figure 4.4: The average specific enthalpy over time using the mixing models IEM, CoDi and MC. The starting conditions are two equal peaks with temperatures 453.16 K and 753.16 K.

When the initial conditions did not start below and above the critical temperature, the mixing models did not have the deviation. This indicates that the critical temperature has something to do with it. Remember figure 1.6, the function consists of two linear sections and one jump in specific enthalpy at the pseudocritical temperature. At T_c a small change in temperature results in a large change in specific enthalpy and the other way around: A large change in enthalpy does not change the temperature by a large amount at T_c. The specific enthalpy is taken as independent variable, so the particles which have a specific enthalpy between 2000 and 2500 kJ/kg are almost at the same temperature. Thus it does not matter if a particle has a specific enthalpy of 2000 kJ/kg or 2500 kJ/kg, its contribution to the average temperature stays the same. IEM keeps the peaks from the initial distribution and moves them to the average. When one of the peaks would get in the regime of the pseudocritical temperature, the temperature of half of the particles stays approximately the same. The other half of the particles keeps moving to the average while outside of the critical temperature regime. This leads to a scenario where one of the peaks is increasing the average temperature, while the other peak is not decreasing it. This is exactly what is happening in the third case. In the first two cases this was not the case, because the distributions would never get close to the critical temperature.

In the third case the average specific enthalpy corresponds to a temperature at the lower part of the critical temperature regime. Regardless of how the mixing will happen, after a long time all particles would be close to this temperature. Particles from the left peak will likely stay left of the final temperature and particles from the right peak will likely stay right. The particles in the critical temperature regime are much more likely coming from the right peak. There is a much larger part of this regime at the right side of the final temperature than left side. So with these starting conditions, of the particles that are located inside the critical temperature regime, there are more particles from the right peak than from the left peak. Equivalently there are more particles outside the regime from the left peak. So whenever there are a lot particles inside the regime but also a lot outside of it, the average temperature will increase fast.

To support these statements a few density functions, at different time steps, of the results from the IEM model are shown.

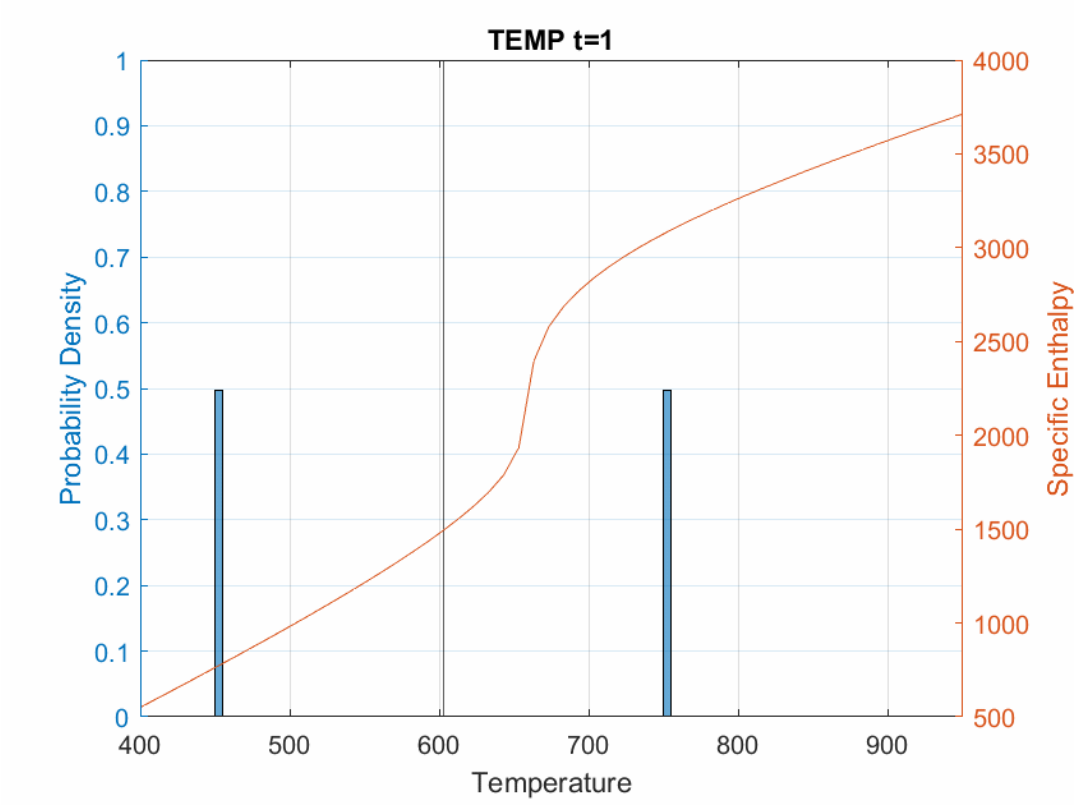
TEMP t=1
Probability Density
Specific Enthalpy
Temperature
0
0.1
0.2
0.3
0.4
0.5
0.6
0.7
0.8
0.9
1
500
1000
1500
2000
2500
3000
3500
4000
400
500
600
700
800
900

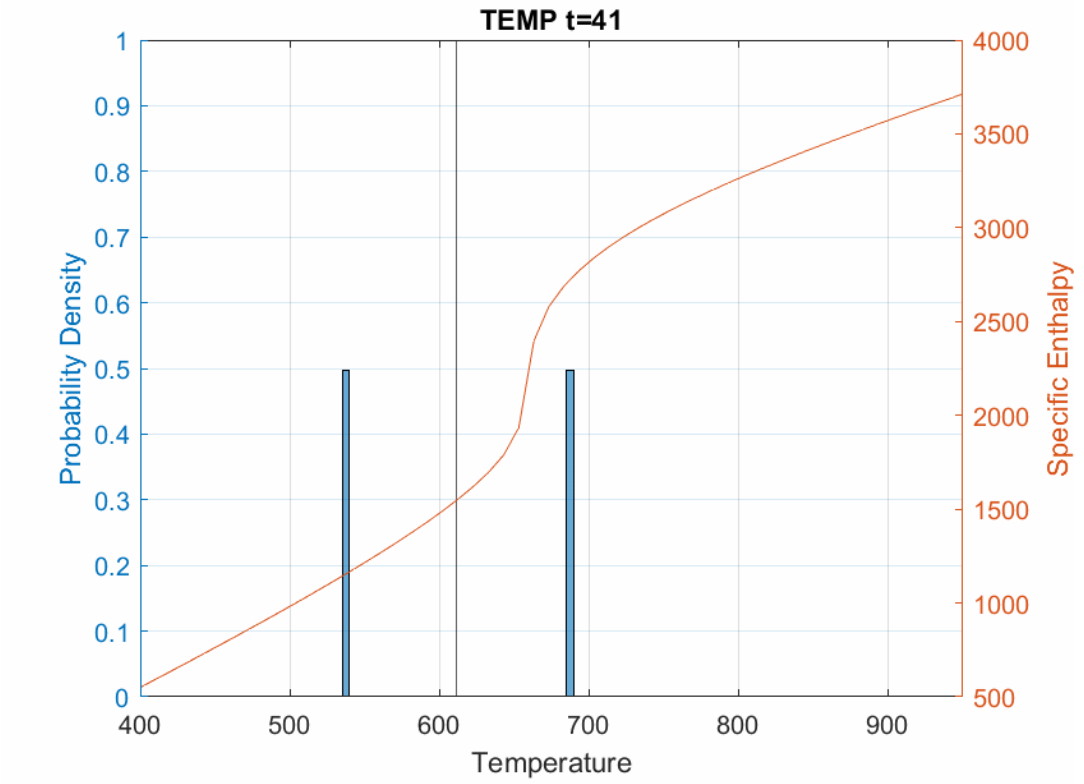
TEMP t=41
Probability Density
Specific Enthalpy
Temperature
0
0.1
0.2
0.3
0.4
0.5
0.6
0.7
0.8
0.9
1
500
1000
1500
2000
2500
3000
3500
4000
400
500
600
700
800
900

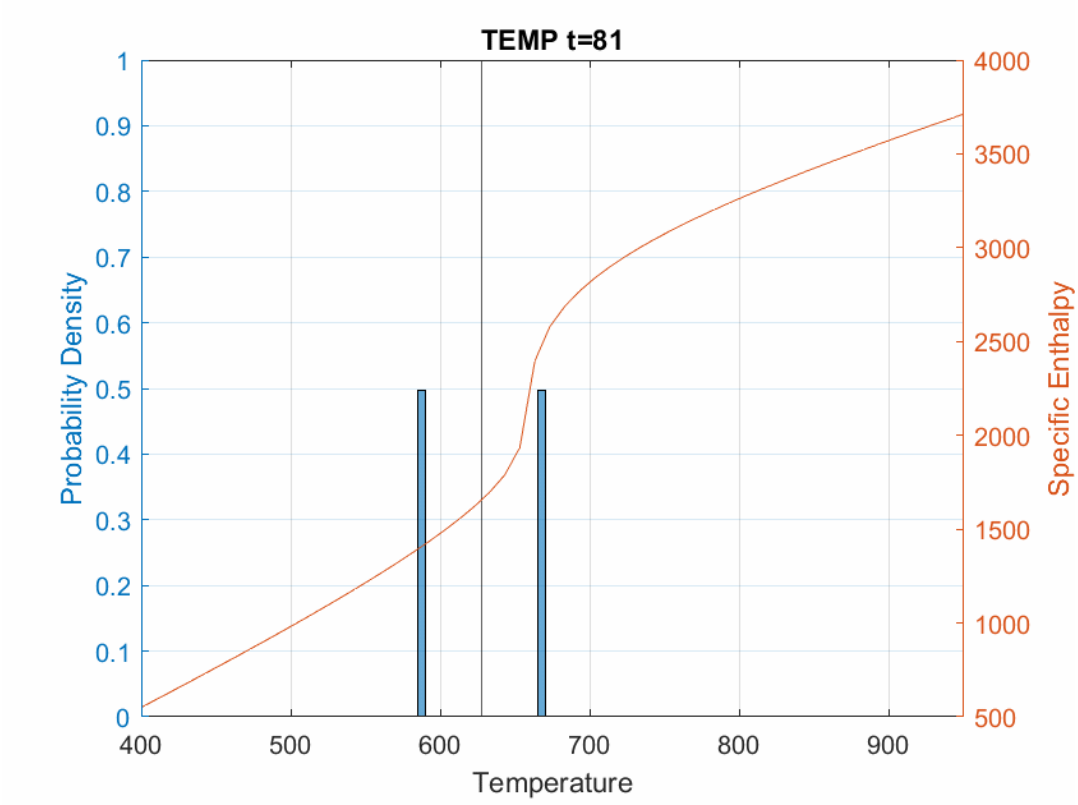
TEMP t=81
Probability Density
Specific Enthalpy
Temperature
0
0.1
0.2
0.3
0.4
0.5
0.6
0.7
0.8
0.9
1
500
1000
1500
2000
2500
3000
3500
4000
400
500
600
700
800
900

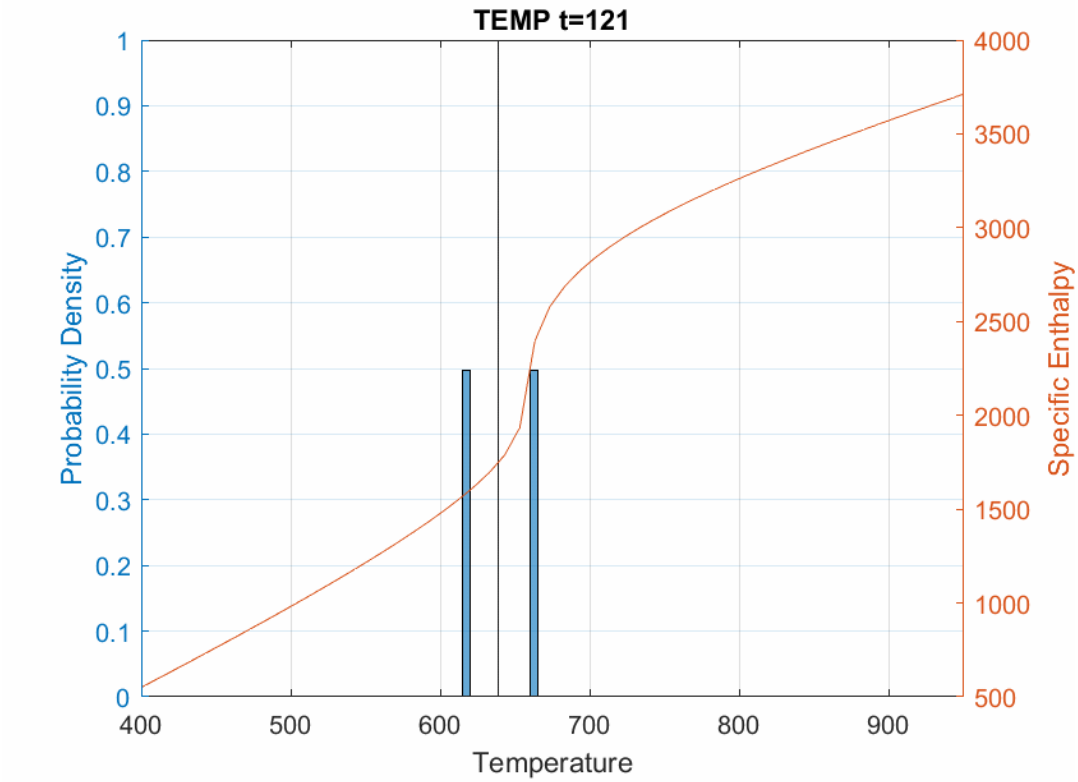
TEMP t=121
Probability Density
Specific Enthalpy
Temperature
0
0.1
0.2
0.3
0.4
0.5
0.6
0.7
0.8
0.9
1
500
1000
1500
2000
2500
3000
3500
4000
400
500
600
700
800
900

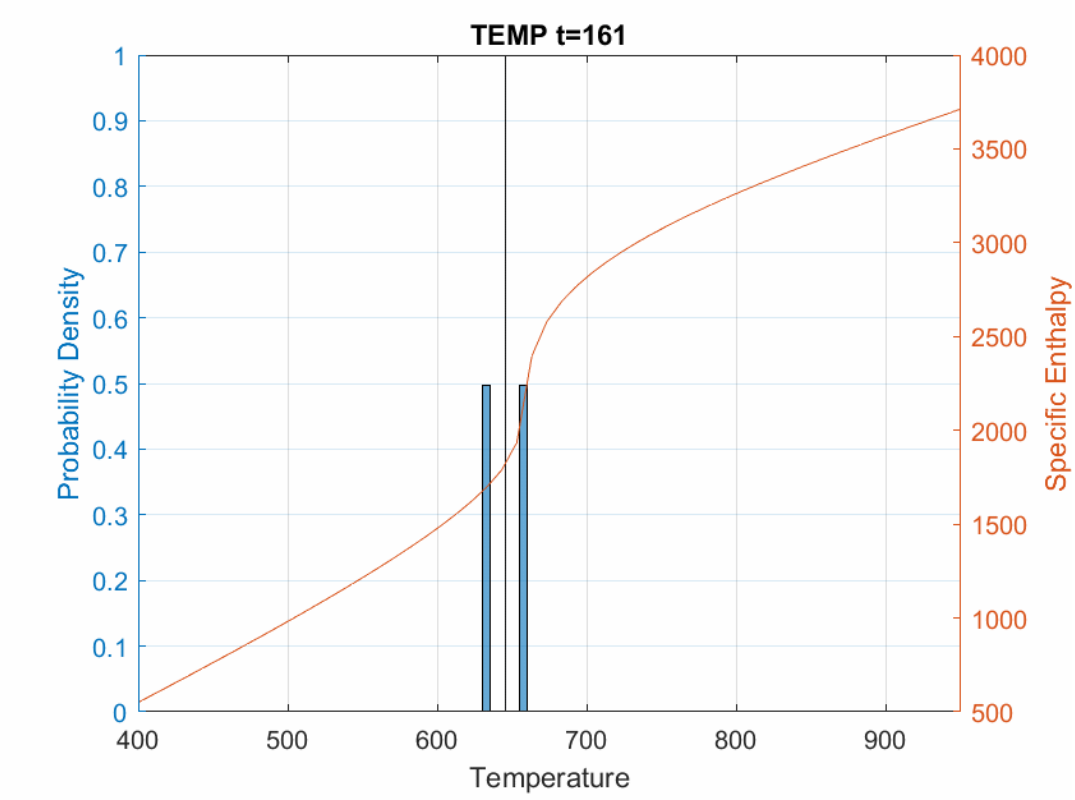
TEMP t=161
Probability Density
Specific Enthalpy
Temperature
0
0.1
0.2
0.3
0.4
0.5
0.6
0.7
0.8
0.9
1
500
1000
1500
2000
2500
3000
3500
4000
400
500
600
700
800
900

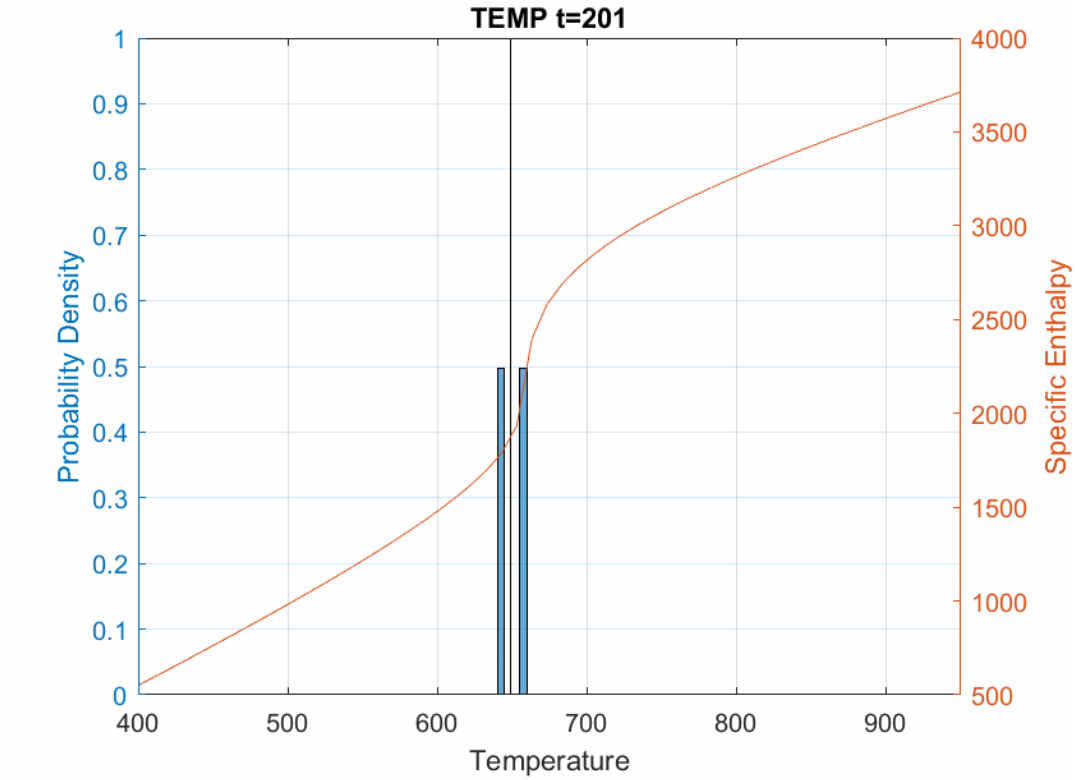
TEMP t=201
Probability Density
Specific Enthalpy
Temperature
0
0.1
0.2
0.3
0.4
0.5
0.6
0.7
0.8
0.9
1
500
1000
1500
2000
2500
3000
3500
4000
400
500
600
700
800
900

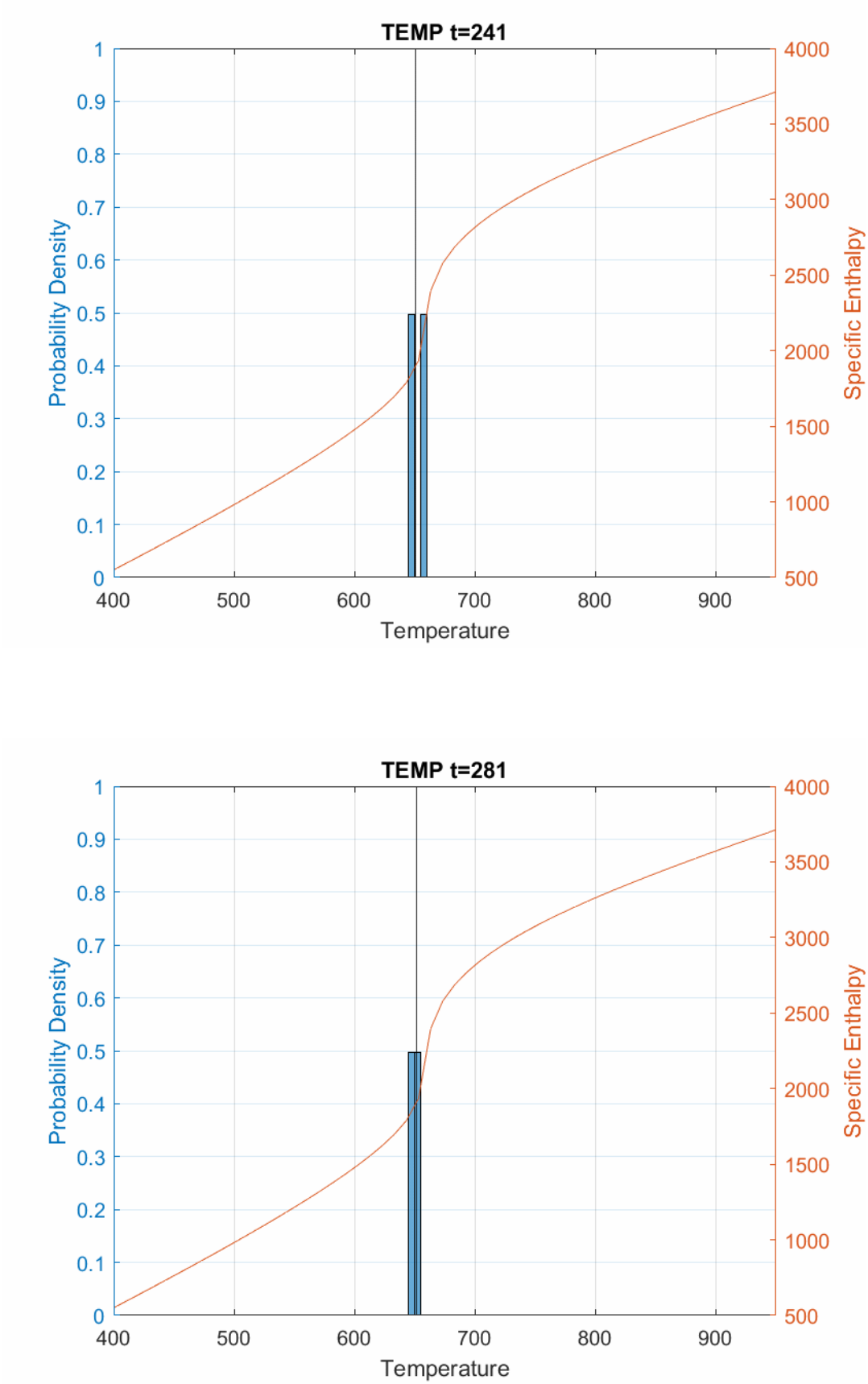

Figure 4.5: Probability density functions at different time steps using the IEM model. The left axis and the bars correspond to the PDF, the right axis and the curved red line correspond to the specific enthalpy. The vertical black line indicates the average temperature.

First the peaks move to the average with comparable speed. Then when the right peak moves close to the pseudocritical temperature it slows a lot down. The left moving peak keeps going to the right without being affected by the pseudocritical temperature. Finally the peaks meet at the average specific enthalpy.

At the first time steps there are no particles in the critical temperature regime, this is why the average temperature increases slow as shown on figure 4.3. Later when the full right peak is inside the regime, the average temperature starts to catch back up to those of the other models.

CoDi and the Mapping Closure model are different for the first steps. Figure 4.6 contains the first steps using the Coalescence Dispersion model and figure 4.7 contains those using the Mapping Closure model.

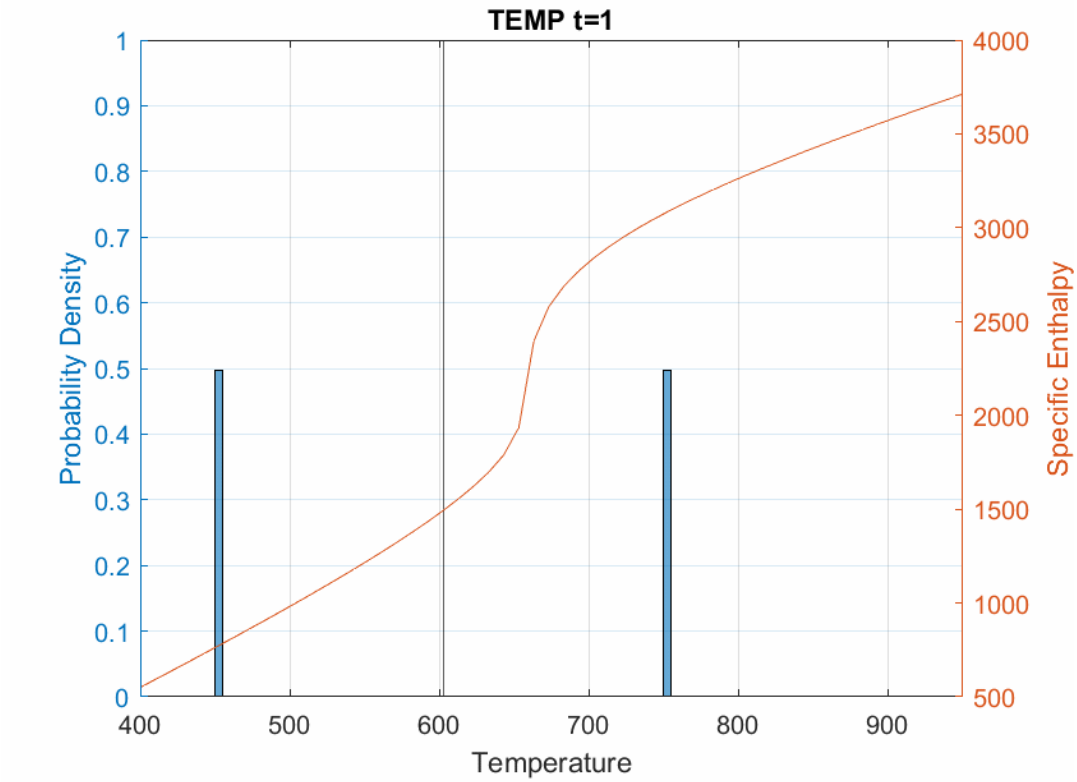

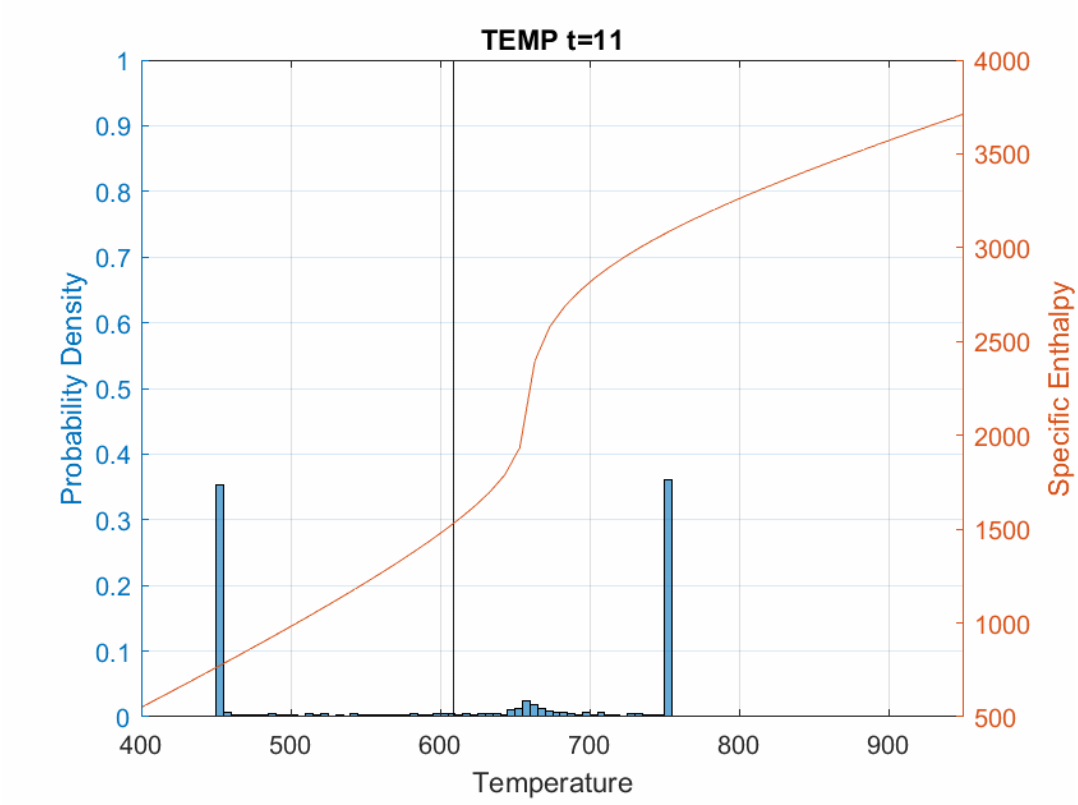
TEMP t=11
Probability Density
Specific Enthalpy
Temperature
0
0.1
0.2
0.3
0.4
0.5
0.6
0.7
0.8
0.9
1
500
1000
1500
2000
2500
3000
3500
4000
400
500
600
700
800
900

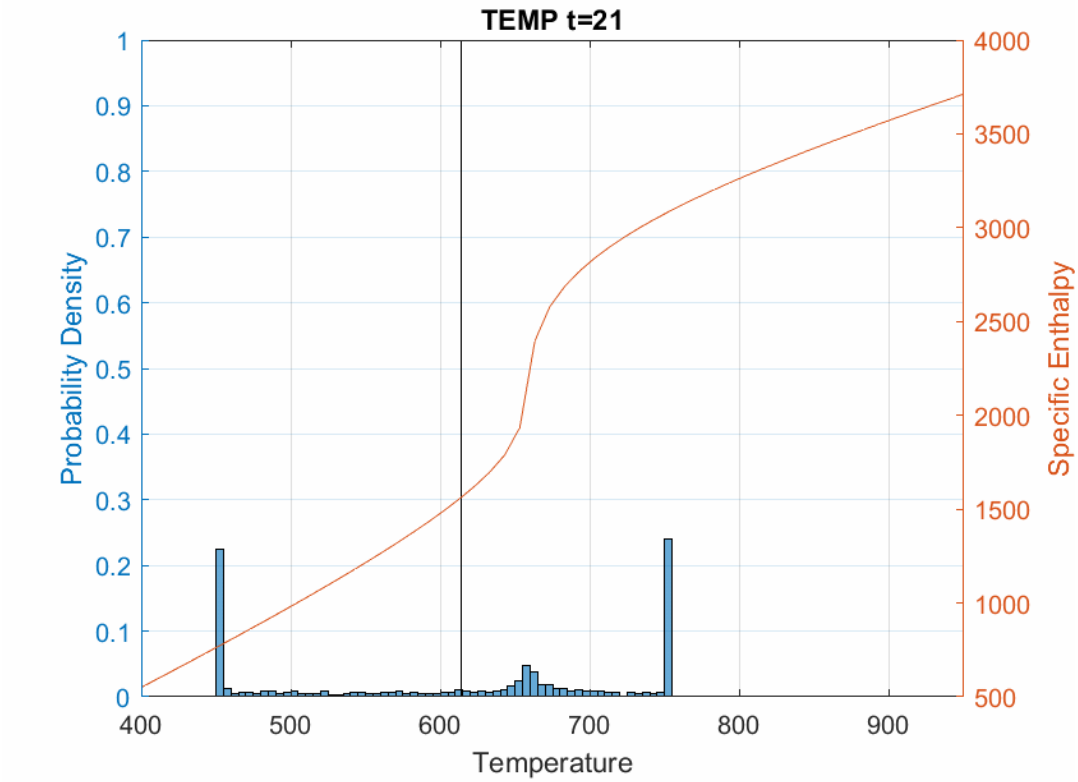
TEMP t=21
Probability Density
Specific Enthalpy
Temperature
0
0.1
0.2
0.3
0.4
0.5
0.6
0.7
0.8
0.9
1
500
1000
1500
2000
2500
3000
3500
4000
400
500
600
700
800
900

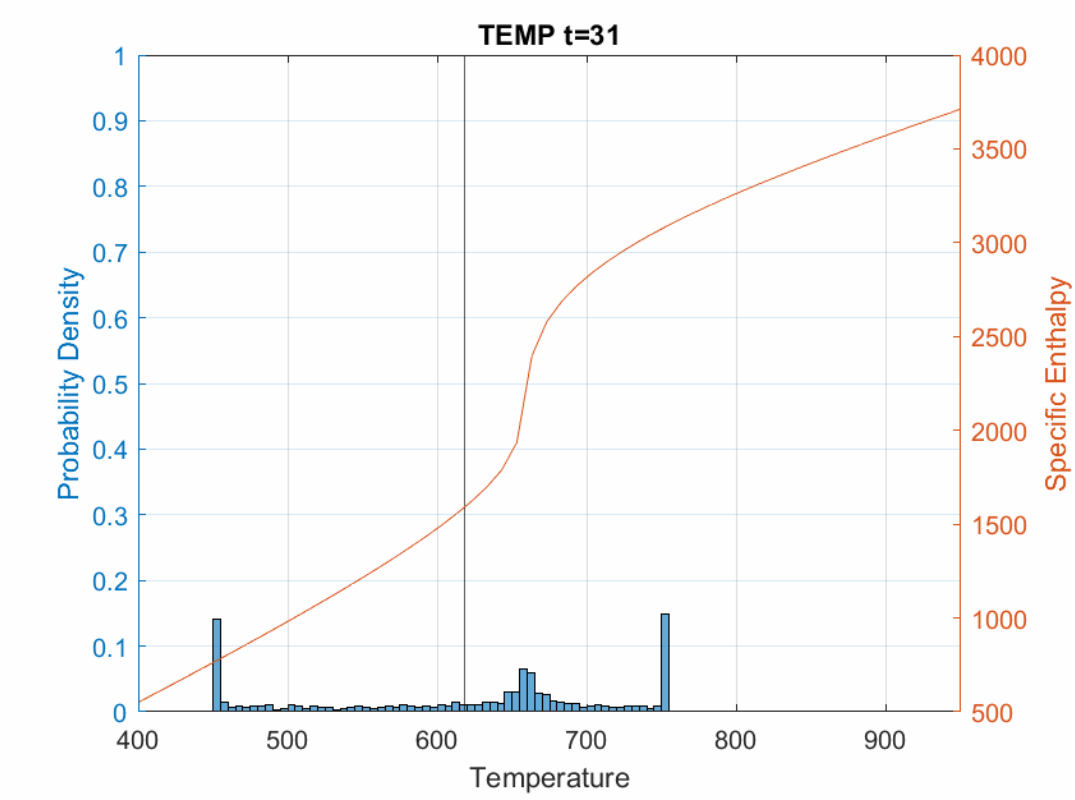
TEMP t=31
Probability Density
Specific Enthalpy
Temperature
0
0.1
0.2
0.3
0.4
0.5
0.6
0.7
0.8
0.9
1
500
1000
1500
2000
2500
3000
3500
4000
400
500
600
700
800
900

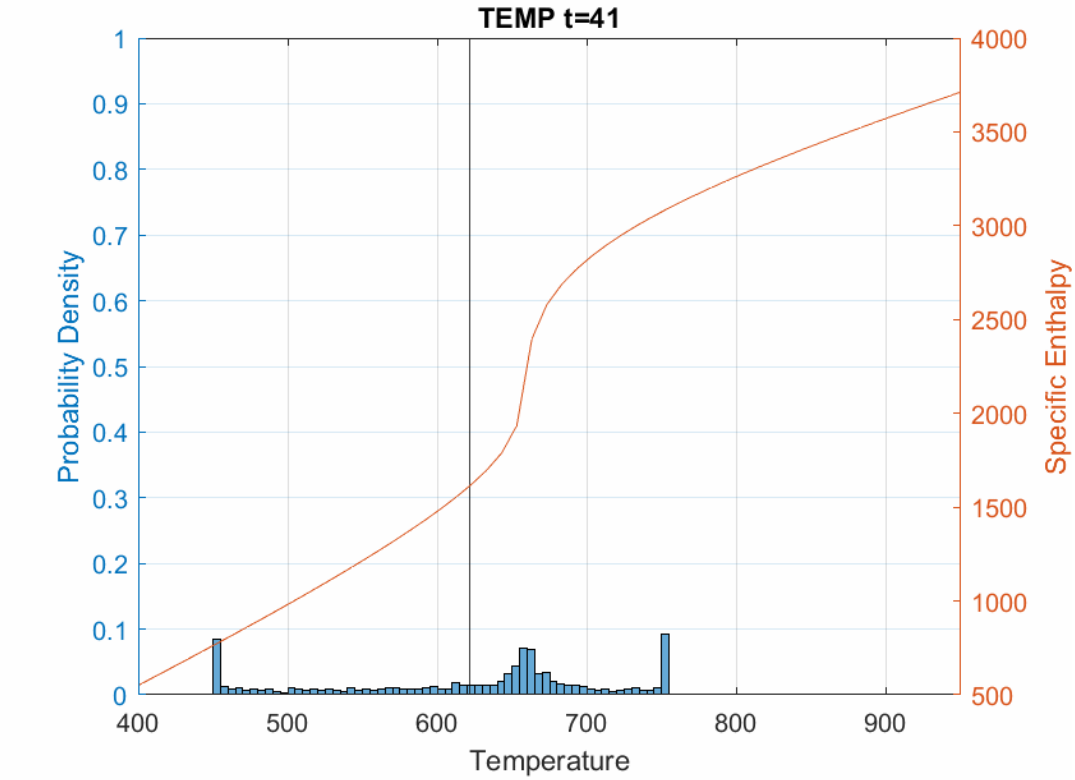
TEMP t=41
Probability Density
Specific Enthalpy
Temperature
0
0.1
0.2
0.3
0.4
0.5
0.6
0.7
0.8
0.9
1
500
1000
1500
2000
2500
3000
3500
4000
400
500
600
700
800
900

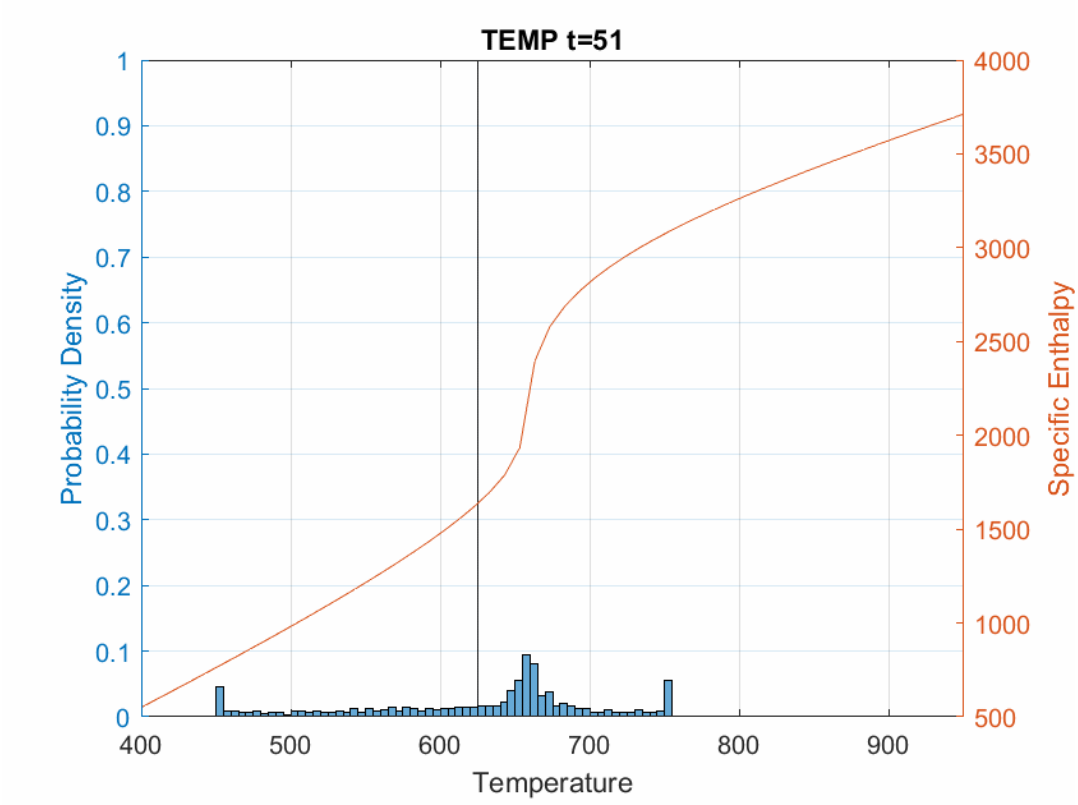

Figure 4.6: Probability density functions at different time steps using the CoDi model. The left axis and the bars correspond to the PDF, the right axis and the curved red line correspond to the specific enthalpy. The vertical black line indicates the average temperature.

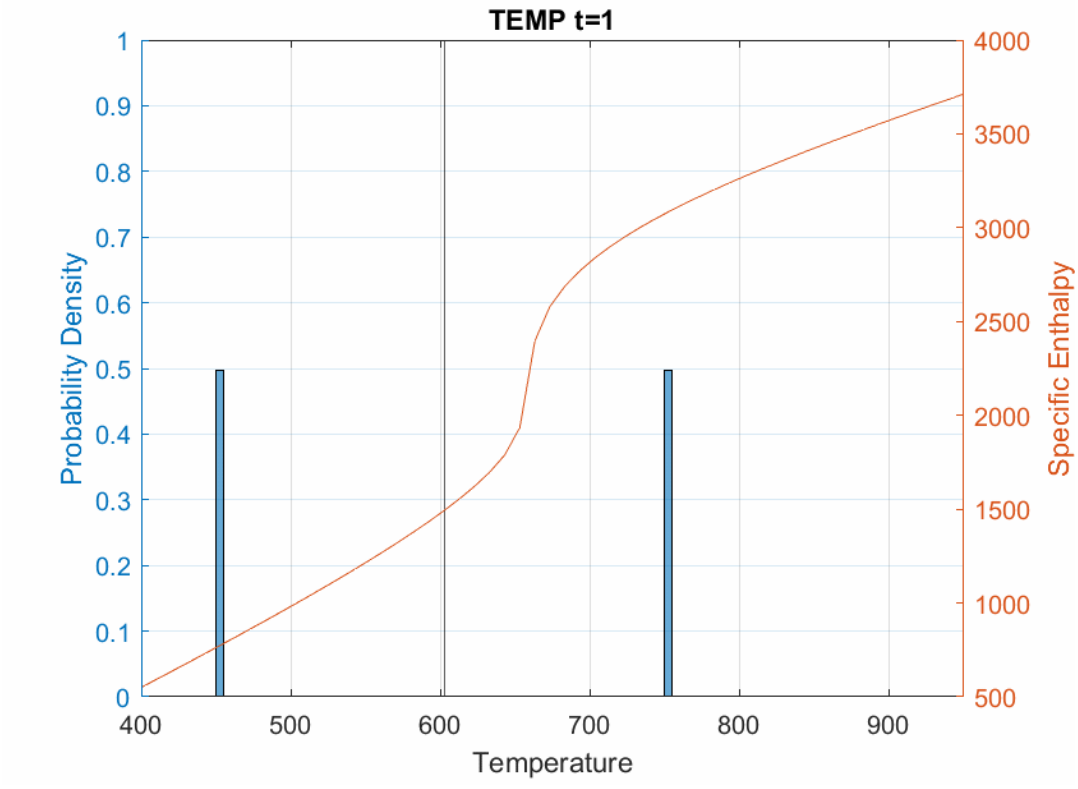

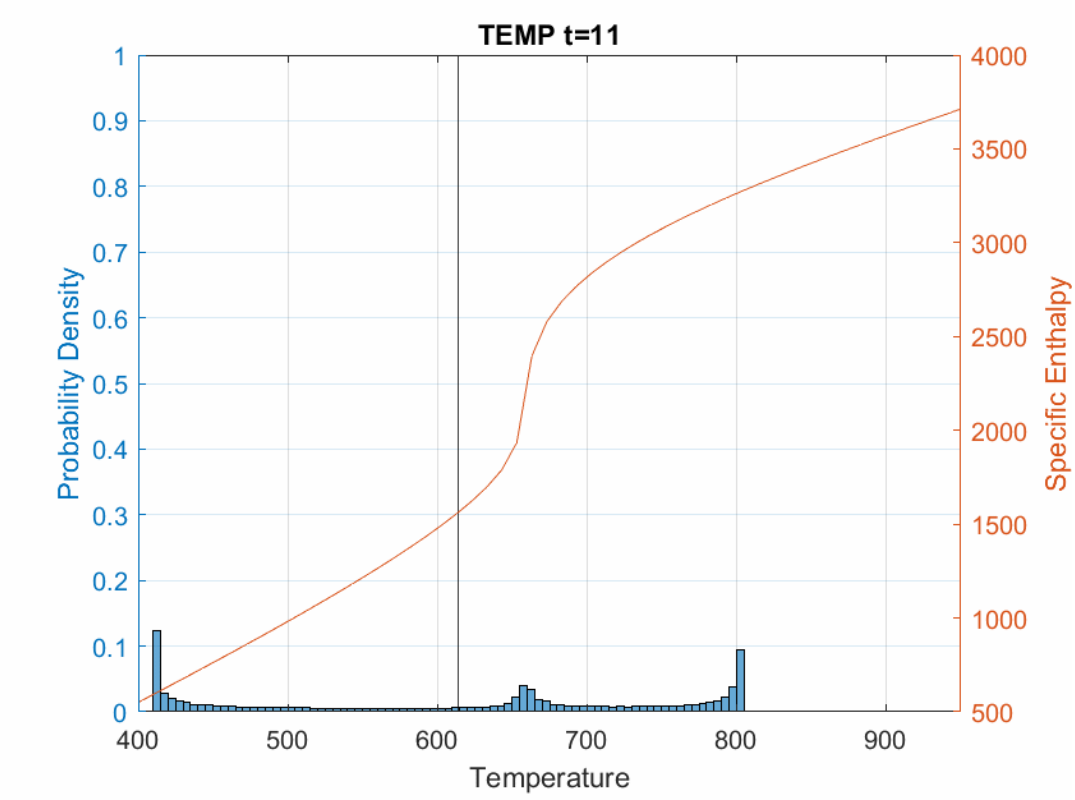
TEMP t=11
Probability Density
Specific Enthalpy
Temperature
0
0.1
0.2
0.3
0.4
0.5
0.6
0.7
0.8
0.9
1
500
1000
1500
2000
2500
3000
3500
4000
400
500
600
700
800
900

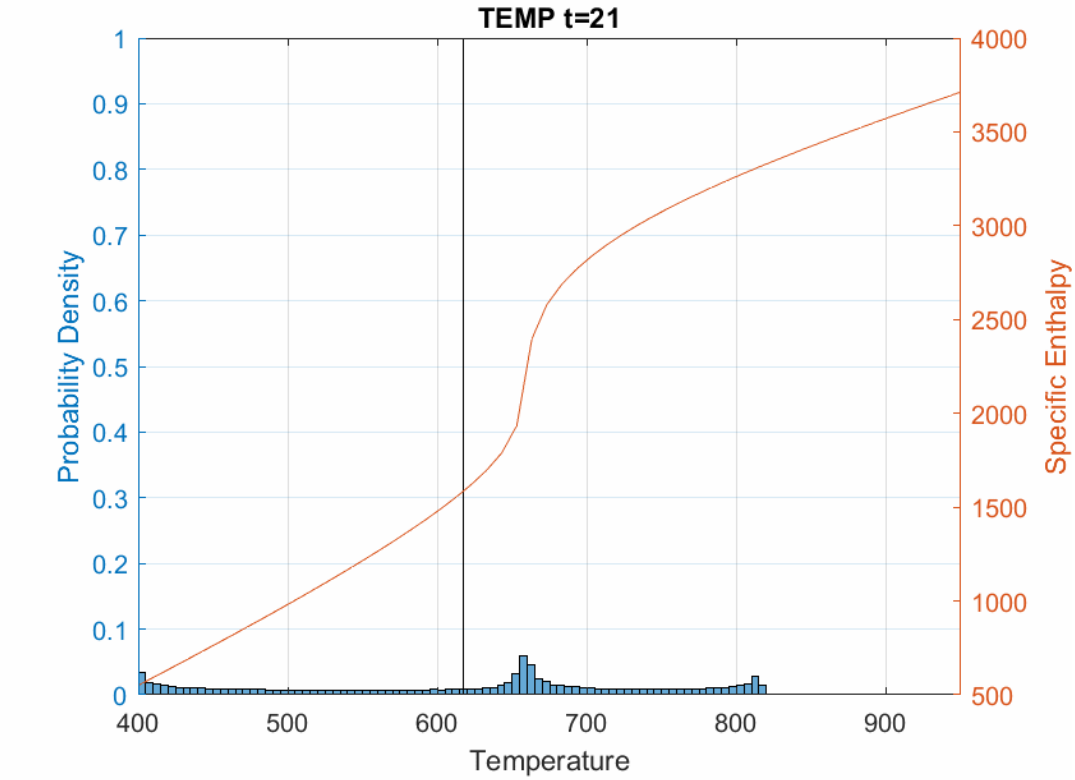
TEMP t=21
Probability Density
Specific Enthalpy
Temperature
0
0.1
0.2
0.3
0.4
0.5
0.6
0.7
0.8
0.9
1
500
1000
1500
2000
2500
3000
3500
4000
400
500
600
700
800
900

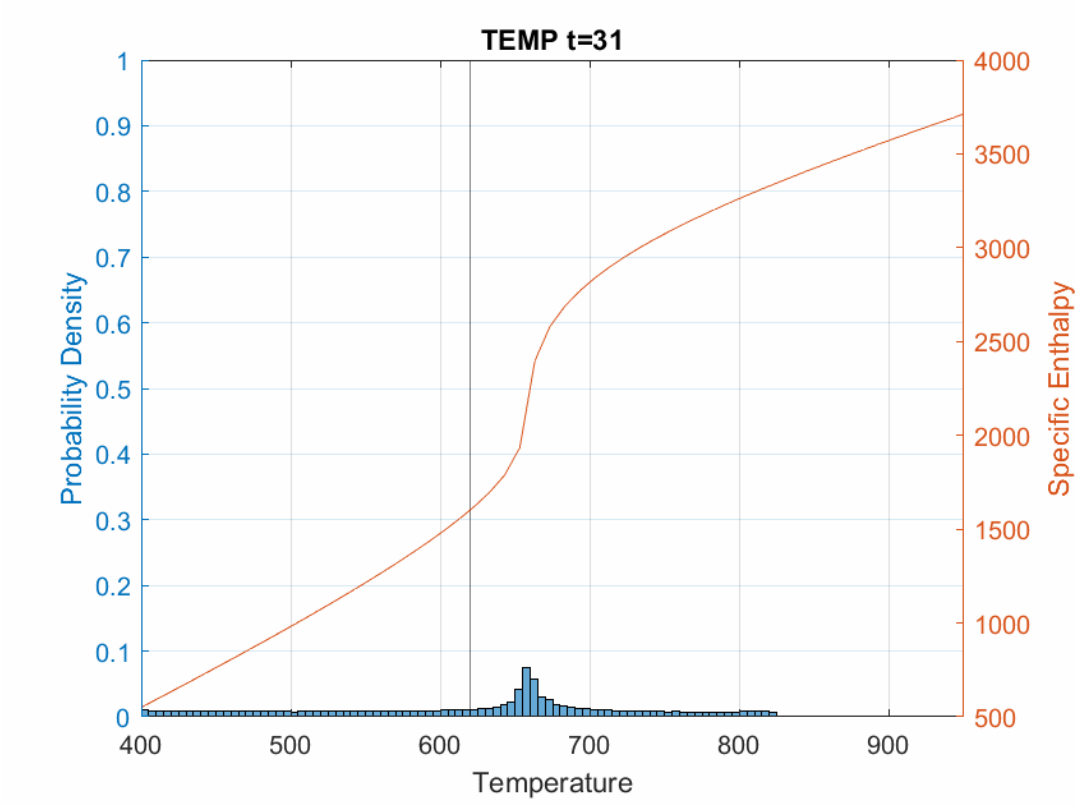
TEMP t=31
Probability Density
Specific Enthalpy
Temperature
0
0.1
0.2
0.3
0.4
0.5
0.6
0.7
0.8
0.9
1
500
1000
1500
2000
2500
3000
3500
4000
400
500
600
700
800
900

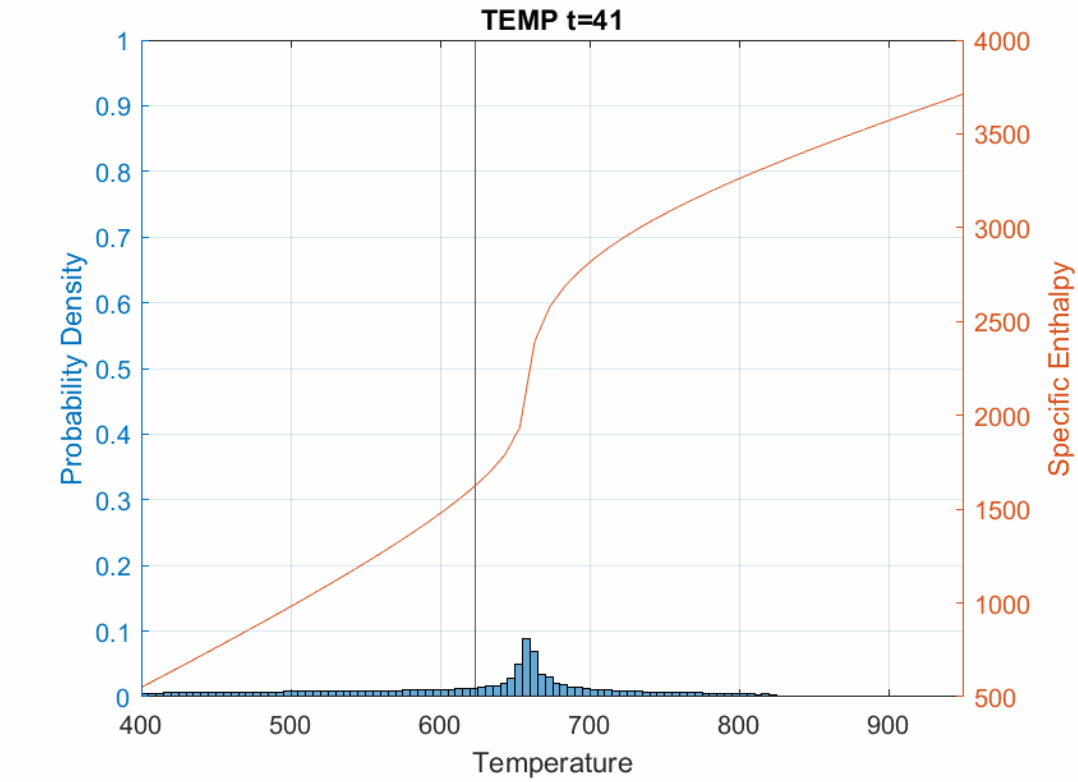
TEMP t=41
Probability Density
Specific Enthalpy
Temperature
0
0.1
0.2
0.3
0.4
0.5
0.6
0.7
0.8
0.9
1
500
1000
1500
2000
2500
3000
3500
4000
400
500
600
700
800
900

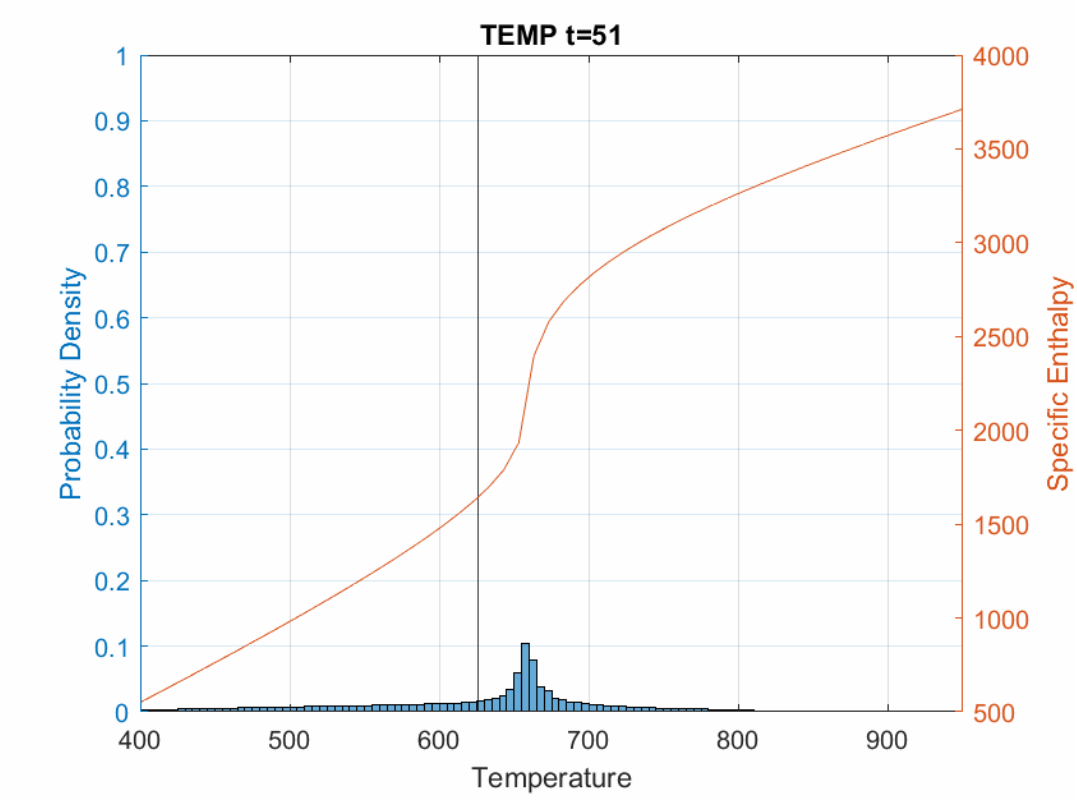

Figure 4.7: Probability density functions at different time steps using the MC model. The left axis and the bars correspond to the PDF, the right axis and the curved red line correspond to the specific enthalpy. The vertical black line indicates the average temperature.

The difference between CoDi and MC is best visible in the figures of $t = 11$. MC has more particles around the pseudocritical temperature than CoDi at this step. This means that the average temperature should increase faster in the results from the MC model compared to those of the CoDi model. Figure 4.3 does indeed show an increased average temperature at t=11 for the Mapping Closure model.

In the first two cases the initial conditions were either both below or above the pseudocritical temperature. At those regions the specific enthalpy is almost linear. That is why the average temperature does not change that much. If the specific enthalpy curve would be perfectly linear the average temperature would not have changed at all. A proof for this is given below.

The temperature $T^{(i)}$ of a particle i depends on a function $g(h^{(i)})$ where g is a function describing the relation between the specific enthalpy and the temperature and $h^{(i)}$ is the specific enthalpy of particle i. The average temperature is defined as:

$\bar{T}(t) \equiv \frac{1}{N}\sum_{i=1}^{N} T^{(i)}(t) = \frac{1}{N}\sum_{i=1}^{N} g(h^{(i)}(t))$

if g would be linear this leads to:

$$\begin{aligned}\bar{T}(t) &= \frac{1}{N}\sum_{i=1}^{N} \alpha h^{(i)}(t) + \beta \\ &= \frac{1}{N}\sum_{i=1}^{N} \alpha h^{(i)}(t) + \frac{1}{N}\sum_{i=1}^{N} \beta \\ &= \frac{\alpha}{N}\sum_{i=1}^{N} h^{(i)}(t) + \frac{\beta}{N}\sum_{i=1}^{N} \\ &= \alpha\bar{h}(t) + \beta\end{aligned}$$

Since the average specific enthalpy does not depend on time: $\bar{h}(t) = \bar{h}$ thus $\bar{T}(t) = \alpha\bar{h} + \beta$ does also not depend on time. In other words: it stays constant.

5

Conclusion

In this report simulations of the mixing of water around the supercritical temperature have been used to get insight in the difference of the three micro mixing models; Interaction by Exchange with the Mean, Coalescence/Dispersion and the Mapping Closure model. The simulations started with two peaks with a different temperature representing two parts of water, one with a smaller temperature than the other. The most important result is that, only when the mixing occurs around the pseudocritical temperature, the average temperature is described differently for the models. IEM had a large deviation from both CoDi and MC. CoDi and MC only deviated at the first steps. The reason for this large deviation in prediction is a difference in mixing scenarios. The enthalpy distribution is different for the models. Together with a nonlinear dependency of specific heat on temperature, this led to a different temperature distribution, and thus a different average temperature. When the mixing occurs far above or far below the pseudocritical temperature all three mixing models have a similar evolution of average temperature.

The Mapping Closure model is best in agreement with the Navier-Stokes equations [16] so when mixing occurs around the pseudocritical temperature it is strongly advised to use a Mapping Closure model instead of IEM or CoDi. For mixing processes which do not come close to this rapid change in properties all three models give the same average temperature.

Water is the most dominant phase inside hydrothermal flames so these results for mixing water should be closely related to the mixing inside a hydrothermal flame environment.

Future research could be done about other micro mixing models. It would also be interesting if the micro mixing is extended to the hydrothermal flame environment with fuel and oxidizer and reaction processes. Then the full flame could be simulated to get a better view on supercritical water oxidation.

A

Appendix

A.1. Derivation of equation 2.5

Starting from:

$$\frac{d\psi^{(i)}(t)}{dt} = -\frac{c\omega}{2}\left(\psi^{(i)}(t) - \frac{1}{N}\sum_{j=1}^{N}\psi^{(j)}(t_0)\right)$$

Writing the average as $\bar{\psi}$ to make it better readable:

$$\frac{d\psi^{(i)}(t)}{dt} = -\frac{c\omega}{2}(\psi^{(i)}(t) - \bar{\psi})$$

$$\frac{d\psi^{(i)}(t)}{dt} = -\frac{c\omega}{2}\psi^{(i)}(t) + \frac{c\omega}{2}\bar{\psi} \quad (*)$$

$$\frac{d\psi^{(i)}(t)}{dt} = -\frac{c\omega}{2}\psi^{(i)}(t) \quad \text{For the homogeneous solution}$$

$$\frac{1}{\psi^{(i)}(t)}d\psi^{(i)}(t) = -\frac{c\omega}{2}dt$$

$$\psi^{(i)}(t) = A(t)e^{-\frac{c\omega}{2}t} \quad (**)$$

$$\frac{d\psi^{(i)}(t)}{dt} = \frac{A(t)}{dt}e^{-\frac{c\omega}{2}t} - \frac{c\omega}{2}A(t)e^{-\frac{c\omega}{2}t}$$

$$\frac{d\psi^{(i)}(t)}{dt} = \frac{A(t)}{dt}e^{-\frac{c\omega}{2}t} - \frac{c\omega}{2}\psi^{(i)}(t) \quad \text{Substituting this into (*)}$$

$$\frac{A(t)}{dt}e^{-\frac{c\omega}{2}t} - \frac{c\omega}{2}\psi^{(i)}(t) = -\frac{c\omega}{2}\psi^{(i)}(t) + \frac{c\omega}{2}\bar{\psi}$$

$$\frac{A(t)}{dt}e^{-\frac{c\omega}{2}t} = \frac{c\omega}{2}\bar{\psi}$$

$$\frac{A(t)}{dt} = \frac{c\omega}{2}\bar{\psi}e^{\frac{c\omega}{2}t}$$

$$A(t) = \bar{\psi}e^{\frac{c\omega}{2}t} + B \quad \text{Substituting this into (**)}$$

$$\psi^{(i)}(t) = \bar{\psi}e^{\frac{c\omega}{2}t}e^{-\frac{c\omega}{2}t} + Be^{-\frac{c\omega}{2}t}$$

$$\psi^{(i)}(t) = \bar{\psi} + Be^{-\frac{c\omega}{2}t} \quad (***)$$

$$\psi^{(i)}(t_0) = \bar{\psi} + Be^{-\frac{c\omega}{2}t_0}$$

$$\psi^{(i)}(t_0) - \bar{\psi} = Be^{-\frac{c\omega}{2}t_0}$$

$$B = e^{\frac{c\omega}{2}t_0}(\psi^{(i)}(t_0) - \bar{\psi}) \quad \text{Substituting this into (***)}$$

$$\psi^{(i)}(t) = \bar{\psi} + e^{-\frac{c\omega}{2}(t-t_0)}(\psi^{(i)}(t_0) - \bar{\psi})$$

$$\psi^{(i)}(t) = e^{-\frac{c\omega}{2}(t-t_0)}\psi^{(i)}(t_0) + \left(1 - e^{-\frac{c\omega}{2}(t-t_0)}\right)\bar{\psi}$$

$$\psi^{(i)}(t) = e^{-\frac{c\omega}{2}(t-t_0)}\psi^{(i)}(t_0) + \left(1 - e^{-\frac{c\omega}{2}(t-t_0)}\right)\frac{1}{N}\sum_{j=1}^{N}\psi^{(j)}(t_0)$$

A.2. Compiling MM-INTAS

Fortran is a programming language well suited for scientific computations. The code is written in text files which need to be compiled in order to get an executable which is essentially the program. The compiling is done by special compiling programs for Fortran such as ifort from Intel or a g95 made by Andy Vaught which I have used during the project.

By writing larger Fortran programs multiple text files are recommended for readability. Compiling multiple files however is a bit more difficult. One way would be to manually compile every file and then link them together. This is however a tedious task. To compiling a single file you would have to type something like: $g95\ \text{-}c\ \ ..\backslash mm\text{-}intas\backslash program\backslash src\backslash files\_module.f90$ in a Command Promt. Doing this after every modification takes a long time, so a new file called Makefile which does these things for you is used. For every file in your program there is a line to compile that file and at the end there is a line which links all the created files to one executable. To make everything even more easy there is a program which makes the Makefile. This file finds every Fortran file (with extention .f90) and then creates a line in the Makefile to compile it. With this new file editing the Makefile is not required after you add more files to your Fortran program.

Linking the files together was difficult, there are a few things to keep in mind. When using the g95 compiler it is important that every object file for your program is inside the link statement, this includes the main file. Also the name of the created executable should exist in the statement and needs to be different from the

names of the other files. For a two file program you could do the linking with *g95 -o mainprogram main.o sub.o*, after you created the two object files by compiling them individually. Something to keep in mind is that long files names could create problems, so keeping the length of the name below 15 characters is advised.

Bibliography

[1] MATLAB Release 2017a, The MathWorks, Inc., Natick, Massachusetts, United States.

[2] F. McMurry. (2004). *Chemistry*. 4th ed. Upper Saddle River, NJ: Pearson Prentice Hall.

[3] C. Augustine and J. Tester. (2009), Hydrothermal flames: From phenomenological experimental demonstrations to quantitative understanding. *The Journal of Supercritical Fluids*, 47(3):pp.415–430.

[4] A. Bhave and M. Kraft. (2004). Partially Stirred Reactor Model: Analytical Solutions and Numerical Convergence Study of a PDF/Monte Carlo Method. *SIAM Journal on Scientific Computing*, 25(5):pp.1798–1823.

[5] M.O. McLinden E.W. Lemmon and D.G. Friend. "Thermophysical Properties of Fluid Systems" in NIST Chemistry WebBook, NIST Standard Reference Database Number 69, Eds. P.J. Linstrom and W.G. Mallard, National Institute of Standards and Technology, Gaithersburg MD, 20899, doi:10.18434/T4D303, (retrieved March 8, 2018).

[6] IAPWS. Release on the Values of Temperature, Pressure and Density of Ordinary and Heavy Water Substances at Their Respective Critical Points. (1992). Available from: http://www.iapws.org.

[7] K. Kuo and R. Acharya. *Fundamentals of turbulent and multiphase combustion*. Hoboken, N.J.: Wiley, (2012).

[8] B.E. Launder and D.B. Spalding. (1974). The numerical computation of turbulent flows. *Computer Methods in Applied Mechanics and Engineering*, 3(2):pp.269–289.

[9] B. Naud and D. Roekaerts. *TEST OF TURBULENT MIXING MODELS: PROGRAM MM-INTAS*, February 2003. URL `http://www.sandia.gov/TNF/mixing.html`.

[10] S. B. Pope. Mapping closures for turbulent mixing and reaction. *Theoretical and Computational Fluid Dynamics*, 2(5):255–270, Aug 1991. ISSN 1432-2250. doi: 10.1007/BF00271466. URL `https://doi.org/10.1007/BF00271466`.

[11] Karol Príkopský. Characterization of continuous diffusion flames in supercritical water, Doctor of Technical Sciences Thesis, Swiss Federal Institue of Technology. (2007). Available from: www.e-collection.ethz.ch.

[12] D. Roekaerts. (1991). Use of a Monte Carlo PDF method in a study of the influence of turbulent fluctuations on selectivity in a jet-stirred reactor. *Applied Scientific Research*, 48(3-4):pp.271–300.

[13] D. Roekaerts and T. Peeters. *Turbulente reagerende stromingen*. Delft: TU Delft, Faculteit der Technische Natuurkunde, (1997).

[14] Teresa Parra-Santos M. García-Serna J. Castro F. Sierra-Pallares, J. and M. José Cocero. (2009). Numerical modelling of hydrothermal flames. Micromixing effects over turbulent reaction rates. *The Journal of Supercritical Fluids*, 50(2):pp.146–154.

[15] S. Subramaniam and S. Pope. (1998). A mixing model for turbulent reactive flows based on Euclidean minimum spanning trees. *Combustion and Flame*, 115(4):pp.487–514.

[16] Ros J. Valiño, L. and C. Dopazo. (1991). Monte Carlo implementation and analytic solution of an inert-scalar turbulent-mixing test problem using a mapping closure. *Physics of Fluids A: Fluid Dynamics*, 3(9): pp.2191–2198.